# Chloride(HCl/Cl⁻) dominates inorganic aerosol formation from ammonia in the Indo-Gangetic Plain during winter: Modeling and comparison with observations

Pooja V. Pawar[1,6], Sachin D. Ghude[1], Gaurav Govardhan[1],Prodip Acharja[1], Rachana Kulkarni[2], Rajesh Kumar[3], Baerbel Sinha[4], Vinayak Sinha[4], Chinmay Jena[5], Preeti Gunwani[1], Tapan Kumar Adhya[6], Eiko Nemitz[7], and Mark A. Sutton[7]

[1]Indian Institute of Tropical Meteorology (IITM), Ministry of Earth Sciences, Pune, India
[2]Savitribai Phule Pune University, Pune, India
[3]National Center for Atmospheric Research (NCAR), Boulder, CO, USA
[4]Department of Earth and Environmental Sciences, Indian Institute of Science Education and Research Mohali, Punjab, India
[5]India Meteorological Department (IMD), Ministry of Earth Sciences, Lodhi Road, New Delhi, India
[6]Kalinga Institute of Industrial Technology (KIIT), Bhubaneshwar, India
[7]UK Centre for Ecology & Hydrology (UKCEH), Edinburgh, UK

*Correspondence to*: Sachin D. Ghude (sachinghude@tropmet.res.in)

**Abstract.** The Winter Fog Experiment (WiFEX) was an intensive field campaign conducted at Indira Gandhi International Airport (IGIA) Delhi, India, in the Indo-Gangetic Plain (IGP) during the winter of 2017-2018. Here, we report the first comparison in South Asia of high temporal resolution simulation of ammonia ($NH_3$)along with ammonium ($NH_4^+$) and total $NH_x$ (= $NH_3 + NH_4^+$) using the Weather Research and Forecasting model coupled with chemistry (WRF-Chem) and measurements made using the Monitor for AeRosols and Gases in Ambient Air (MARGA) at the WiFEX research site. In the present study, we incorporated Model for Simulating Aerosol Interactions and Chemistry (MOSAIC) aerosol scheme into the WRF-Chem. Despite simulated total $NH_x$ values/variability often agreed well with the observations, the model frequently simulated higher $NH_3$ and lower $NH_4^+$ concentrations than the observations. Under the winter conditions of high relative humidity (RH) in Delhi, hydrogen chloride (HCl) was found to promote the increase in the particle fraction of $NH_4^+$ (which accounted for 49.5 % of the resolved aerosol in equivalent units) with chloride ($Cl^-$) (29.7 %) as the primary anion. By contrast, the absence of chloride (HCl/$Cl^-$) and their chemistry in the standard WRF-Chem model results in the prediction of sulfate ($SO_4^{2-}$) as the dominant inorganic aerosol anion. To understand the mismatch associated with the fraction of $NH_x$ in the particulate phase ($NH_4^+/NH_x$), we added HCl/$Cl^-$ to the model and evaluated the influence of its chemistry by conducting three sensitivity experiments using the model: No HCl, Base Case HCl (using a published waste burning inventory), and 3×Base HCl run. We found that 3×Base HCl increased the simulated average $NH_4^+$ by 13.1 μg m$^{-3}$ and $NH_x$ by 9.8 μg m$^{-3}$ concentration while reducing the average $NH_3$ by 3.2 μg m$^{-3}$, which is more in accord with the measurements. Thus HCl/$Cl^-$ chemistry in the model increases total $NH_x$ concentration, which was further demonstrated by reducing $NH_3$ emissions by a factor of 3 (-3×$NH_3$_EMI) in the 3×Base HCl simulation. Reducing $NH_3$ emissions in the3×Base HCl simulation successfully addressed the discrepancy between measured and modelled total $NH_x$. We conclude that modelling the fate of $NH_3$ in Delhi requires a correct chemistry mechanism accounting for chloride dynamics with accurate inventories of both $NH_3$ and HCl emissions.

## 1 Introduction

The Indo-Gangetic Plain (IGP)is one of the global hotspots of atmospheric ammonia ($NH_3$) and faces a range of environmental challenges, particularly during the winter season, including adverse air pollution episodes, especially as $NH_3$ plays a substantial role in secondary aerosol formation (Ghude et al., 2020, 2008b, 2008a; Kumar et al., 2021; Saraswati et al., 2019; Sharma et al., 2020; Singh et al., 2021). Atmospheric $NH_3$, along with oxides of nitrogen ($NO_x$), together account for the largest source of reactive nitrogen ($N_r$), which is primarily emitted by agricultural activities, livestock population, industrial activities, and transportation (Ghude et al., 2009, 2010, 2012, 2013; Móring et al., 2021; Pawar et al., 2021; Sutton et al., 2017b). Ammonia in the environment plays a crucial role in atmospheric chemistry and the eutrophication and acidification of ecosystems (Datta et al., 2012; Mandal et al., 2013; Pawar et al., 2021; Sharma et al., 2008, 2012, 2014b). Control of $NH_3$ becomes a key priority in an emerging international strategy to manage the global nitrogen cycle (Gu et al., 2021; Sutton et al., 2020). Ammonia is one of the important aerosol precursor gases, and ammonium ($NH_4^+$) is a major counter ion for the three anions such as chloride ($Cl^-$), nitrate ($NO_3^-$), and sulfate ($SO_4^{2-}$) contributing to $PM_{2.5}$ composition (Seinfeld et al., 2016). In addition, as the dominant alkaline gas in the atmosphere, $NH_3$ has attracted the interest of scientific researchers since it has been known to promote new aerosol formation both in the initial homogeneous nucleation and in the subsequent growth, especially during wintertime (Acharja et al., 2020, 2021; Ali et al., 2019; Duan et al., 2021; Wagh et al., 2021).

In this study, we focus on wintertime since this season is characterized by low-to-dense fog events, lower temperature (T), and variability of relative humidity (RH), which fluctuates from 40 to 100 % (Ghude et al., 2017; Kumar et al., 2020). Ammonia acts as a neutralization agent for determining the acidity of aerosol particles (Acharja et al., 2020; Ali et al., 2019; Ghude et al., 2017). It also affects $PM_{2.5}$, the acidity of clouds, and the wet deposition of nitrogen by neutralizing acidic species (Gu et al., 2021; Xu et al., 2020). Increasing $NH_3$ concentration over Delhi compared with the surrounding area leads to an increase in $PM_{2.5}$ concentrations (Ghude et al., 2022; Sharma et al., 2008, 2012, 2014a), which in turn affects air quality, human health, and climate (Behera et al., 2013; Ghude, 2016; Ghude et al., 2008b; Nivdange et al., 2022; Sutton et al., 2017a; Sutton and Howard, 2018).

Satellite observations (Van Damme et al., 2018; Warner et al., 2017), chemical transport models (CTMs) (Clarisse et al., 2009, 2010; Wang et al., 2020b), and ground-based observations (Pawar et al., 2021) revealed that the IGP is the largest regional hotspot of $NH_3$ concentrations on Earth. Previous studies have identified various sources of $NH_3$, for example, agricultural activities, industrial sectors, motor vehicles, garbage, sewage, and urine from rural populations at the global scale (Behera et al., 2013; Huang et al., 2012; Sutton et al., 2008). However, in Delhi, agricultural activity (including surrounding arable and sub-urban livestock farming) is estimated to be the dominant source of $NH_3$, along with traffic emissions (Kuttippurath et al., 2020; Móring et al., 2021; Sharma et al., 2020), but its emissions are subject to large uncertainty. Globally, various modeling efforts have investigated the relative effectiveness of reducing $NH_3$ emissions in curtailing $PM_{2.5}$ formation (Gu et al., 2021; Pinder et al., 2007, 2008; Zhang et al., 2020). However, over India, the impact on reducing $PM_{2.5}$ might be limited because $NH_3$ emission reductions may be more challenging due to its diverse and area-wide sources. Ianniello et al. (2010) and Lan et al. (2021) have investigated the variation of atmospheric $NH_3$ at an urban and suburban site of Beijing with respect to meteorological factors, where RH was found to be a strong factor in influencing the $NH_3$ mixing ratio. A few studies over Asia have highlighted the

80  gas-to-particle conversion of $NH_3$ in Delhi (Acharja et al., 2021; Saraswati et al., 2019) and China and its

81  subsequent impact on the aerosol formation (Wang et al., 2015; Xu et al., 2020). Furthermore, excess $NH_3$

82  during fog can also enhance secondary aerosol formation in Delhi during winter (Acharja et al., 2021).

83  However, the wintertime behavior of $NH_3$ in Delhi in CTMs has not yet been investigated and remains poorly

84  understood (Ellis et al., 2011; Metzger et al., 2006). In a recent study, Pawar et al. (2021) highlighted

85  uncertainties associated with gas-to-particle partitioning of $NH_3$ in a global model MOZART-4 and found a

86  significant overestimation of $NH_3$ in the model compared with the measurements. The overestimation of $NH_3$ in

87  the model led the authors to hypothesize that a source specific $NH_3$ emission inventory in India, considering

88  agricultural statistics on fertilizer use and animal distribution, was missing. Also, there was a need for a high-

89  resolution regional model with advanced chemistry to resolve the $NH_3$ emissions on the local scale.

90      The present study utilizes the regional Weather Research and Forecasting model coupled with

91  chemistry (WRF-Chem) interpreted using measurements from the Winter fog Experiment (WiFEX), including

92  $NH_3$, water-soluble ions in $PM_{2.5}$, other trace gases, and meteorological parameters during December-January,

93  2017-18. For the first time in South Asia, we discuss and compare the modelled and observed temporal variation

94  in gaseous $NH_3$, particulate $NH_4^+$, and total $NH_x$ (= $NH_3$ + $NH_4^+$). Since we found that the total modelled $NH_x$

95  matches well with the observations, we investigate the ability of the model to accurately describe the gas-to-

96  particle partitioning of the measurements (MARGA) by evaluating the fraction of $NH_x$ in the particulate phase

97  ($NH_4^+/NH_x$). We conducted several sensitivity experiments with and without adding anthropogenic waste

98  burning emissions of hydrochloric acid (HCl) in the model. The updated model with $HCl/Cl^-$ chemistry was used

99  to analyze and compare the temporal variation of $NH_3$, $NH_4^+$, and total $NH_x$ from the WiFEX measurements.

100  **2. Data and methodology**

101  **2.1 Observational datasets**

102  **2.1.1 Description of MARGA**

103      In the present study, we used the same dataset which was previously published by Acharja et al. (2020)

104  and 2021), which described the aerosol time-series and chemistry measured with a Monitor for AeRosols and

105  Gases in Ambient Air-model 2S instrument (MARGA). The MARGA system has two channels, one for

106  sampling $PM_1$ and the other for sampling $PM_{2.5}$ for ground-based observations. The MARGA (two sampling

107  boxes, analytical box, and connected pumps) was located inside the Indira Gandhi International Airport (IGIA),

108  New Delhi (28.56° N, 77.09° E), with the inlet $PM_1$ and $PM_{2.5}$ impactors fixed on the terrace with 2 m long inlet

109  lines sampling outdoor air at 8 m above ground and 2 m above the rooftop. Measurements covered a winter

110  period (19 December 2017 to 21 January 2018) with frequent moderate to dense fog events. Following intake

111  through the $PM_1$ and $PM_{2.5}$ impactors, the air was passed through two parallel inlet tubes 2 m long and 14 mm

112  inner diameter PolyTetraFluoroEthylene (PTFE) to the $PM_1$ and $PM_{2.5}$ sampling channels of the MARGA. The

113  air flow rate in each MARGA sampling box is regulated to a volumetric flow of 1 $m^3$ $h^{-1}$. The measurements are

114  close to real-time, as two sets of syringes are employed to collect the samples in which a set of syringes collects

115  the sample and another set sends the collected samples from the previous hour for analysis. Each MARGA

116  sampling system consists of a steam jet aerosol collector (SJAC) and a wet rotating denuder (WRD) for

collecting and measuring water-soluble inorganic particulate species and gases in the ambient air. The continuous coating of the WRD by a thin film of absorption solution (10 ppm hydrogen peroxide ($H_2O_2$)) allows the diffusion of gases into the absorption solution. By contrast, the low diffusion velocity of sub-micron particles restricts the ability of water-soluble aerosols to diffuse into the absorption solution. The absorption solution is continually changed to replace that abstracted for ion chromatography (IC) analysis of the dissolved gases. The air stream, depleted of gases by the WRD, subsequently enters the SJAC, where the steam enhances water-soluble aerosols to grow, allowing their mechanical capture in a cyclone. The aqueous solutions deriving from two cyclones (for $PM_1$ and $PM_{2.5}$, respectively) are then supplied to the IC for chemical analysis (Acharja et al., 2020).

Ambient surface concentrations of $NH_3$ along with other trace gases (HCl, nitrous acid (HONO), nitric acid ($HNO_3$), and sulfur dioxide ($SO_2$)) and water-soluble inorganic components of $PM_1$ and $PM_{2.5}$ ($Cl^-$, nitrate ($NO_3^-$), $SO_4^{2-}$, $NH_4^+$, sodium ($Na^+$), potassium ($K^+$), magnesium ($Mg^{2+}$), and calcium ($Ca^{2+}$) were then quantified online by anion and cation chromatography in the analytical box at an hourly resolution. We have used only $PM_{2.5}$ inorganic water-soluble components and the gaseous measurements (available from both the $PM_1$ and $PM_{2.5}$ MARGA collection systems). Since $NH_4^+$ with the three major anions: $Cl^-$, $NO_3^-$ and $SO_4^{2-}$ constituted 97.3 % of the total measured ions in $PM_{2.5}$ (Acharja et al., 2020), we consider these four significant ions in our present study. In contrast, the remaining ionic species (i.e., $Na^+$, $K^+$, $Mg^{2+}$ and $Ca^{2+}$) contributed only about 3 % of the total measured ions and were neglected as it would not impact our present study significantly (Acharja et al., 2020). Anions are separated in a MetrosepA Supp-10 (75/4.0) column with sodium carbonate ($Na_2CO_3$) and sodium bi-carbonate ($NaHCO_3$) (7/8 mmol $l^{-1}$) eluent. Whereas for cations separation, a Metrosep C4 (100/4.0) cation column with 3.2 mmol $l^{-1}$ $HNO_3$ eluent was used (Acharja et al., 2020). To suppress the eluent background conductivity of anion chromatographs, three ion exchange units were used to ensure that the ion exchange unit is regenerated in each analysis.1 M Phosphoric acid ($H_3PO_4$) was used for this purpose. This was performed to improve the signal-to-noise (S/N) of the anion chromatographs. Details of the MARGA instrument can be found in Makkonen et al. (2012), Thomas et al. (2009), Twigg et al. (2015).

## 2.1.2 Quality assurance/quality control (QA/QC) of MARGA

To ensure the observation's accuracy and check the data's quality, we have followed best practices during the study. The eluents, absorption, and regenerant solutions were prepared with minimum manual intervention. The operational parameters like anion and cation conductivity, SJAC heater temperature, column oven temperature, and airflow were regularly monitored to keep them within the safe limit. In addition to these, before injection of each sample into the anion and cation IC columns,the Lithium Bromide (LiBr) internal standard solution containing 320 µg $l^{-1}$ lithium ($Li^+$) and 3680 µg $l^{-1}$ bromide ($Br^-$) was mixed with each sample to provide calibration of each analysis. This ensures that each analysis is calibrated, and the concentration of gaseous and ionic samples are measured accurately. The $PM_1$ and $PM_{2.5}$ impactors were typically cleaned fortnightly to remove any material that may have stuck on the surface and inlets of the impactors. The lower detection limits (LODs) of the species monitored by MARGA were mentioned in Acharja et al. (2021). It shows that concentrations of species like $Cl^-$, $NO_3^-$, $SO_4^{2-}$, $NH_4^+$, $SO_2$, and $NH_3$ were always higher than LODs during the winter period. But, concentrations of species like $Na^+$, $K^+$, $Ca^{2+}$, $Mg^{2+}$, HCl, HONO, and $HNO_3$ were sometimes below LODs, but the fraction of it was less than ~10 % of the total observation period. We have omitted these

156  values and treated them as NA. As the fraction of observational hours is less and these species contribute much
157  less to the $PM_1$ and $PM_{2.5}$ mass concentrations, we believe below LODs values would not significantly deviate
158  our results. The quality of the data obtained was then checked using the ion-balance method. As an additional
159  quality check, the ratio of the sum of cations to anions (neq m$^{-3}$) was used as an indicator for the viable data. We
160  have checked the cation-to-anion ratio of each hourly sample expressed in the unit of neq m$^{-3}$. We accepted only
161  those values near to unity and rejected those not within the 10 % error bar limit. Based on this evaluation
162  method, overall, for the campaign, the ratio was near unity (1.06 for $PM_1$ and 0.96 for $PM_{2.5}$). Excellent charge
163  balance between anions and cations measured by the system also confirms that there are no significant
164  contamination issues associated with the aerosol measurements. Values in slight excess of unity may indicate
165  the presence of formate and acetate in the aerosol, which MARGA does not measure. Further detail on the
166  quality control of MARGA can be found in Acharja et al. (2020).

### 2.1.3 Other ground-based measurements

168  Hourly $NO_x$ measurements were made by the chemiluminescence method, and hourly ozone ($O_3$) measurements
169  were made by the UV photometric method (CPCB, 2011) at the nearest air quality monitoring station (AQMS)
170  of IGIA operated by the Central Pollution Control Board (CPCB). CPCB follows the United States
171  Environmental Protection Agency (USEPA) approved AC32M $NO_x$ and 42M $O_3$ analyzer manufactured by
172  Environment S. A. India Private Limited. We used one-hour monitored $NO_x$ and $O_3$ values in our study. These
173  air quality monitoring stations' quality control and assurance processes were followed as outlined in CPCB
174  (2014, 2020). For data quality of CPCB, we omitted all those observed values which fell below LOD of the
175  instrument (2 µg m$^{-3}$ for $NO_x$ and 4 µg m$^{-3}$ for $O_3$) (Technical specifications for CAAQM station, 2019) and
176  above 500 µg m$^{-3}$ for $NO_x$ and 140 µg m$^{-3}$ for $O_3$ and treated them as NA at a given site. For the $NO_x$ and $O_3$
177  datasets, only a small fraction of data (2 %) were outside the instrument operating ranges specified. This step
178  aims to remove any short-term local influence that the models cannot capture and retain the regional-scale
179  variability because the nearest sites are located in the urban environment. We removed a single spike
180  represented by a change of more than 100 µg m$^{-3}$ in just 1 hour (h) for all the data in CPCB monitoring stations
181  to filter out random fluctuations in the observations. We removed some very high $NO_x$ and $O_3$ values that
182  appeared in the time series right after measurement gaps. Meteorological parameters, including air temperature
183  (T), relative humidity (RH), wind speed, and wind direction, were measured with the automatic weather station
184  (AWS) platform on a 20 m flux tower (Ghude et al., 2017). For detailed information on the measurement site
185  and its meteorological parameters, refer to (Ali et al., 2019).

### 2.2 WRF-Chem v 3.9.1 model

187  The Weather Research and Forecasting model coupled with chemistry (WRF-Chem v3.9.1) was employed in
188  this study to simulate atmospheric gases and aerosols over Delhi during the peak winter period, starting from 19
189  December 2017 to 21 January 2018. We recently used a similar model configuration to simulate the air quality
190  over Delhi (Ghude et al., 2020; Kulkarni et al., 2020). This study used the Model for Ozone And Related
191  chemical Tracers (MOZART-4) gas-phase chemical mechanism coupled with the Model for Simulating Aerosol
192  Interactions and Chemistry (MOSAIC) aerosol scheme, that simulates $SO_4^{2-}$, $NH_4^+$, $NO_3^-$, methanesulfonate,
193  $Na^+$, $Ca^{2+}$, $Cl^-$, carbonate, black carbon, and primary organic mass. Other inert minerals, trace elements, and

194 inorganic species are lumped together as different inorganic masses. MOSAIC allows gas-to-particle formation,
195 which includes $NH_3$, HCl, sulfuric acid ($H_2SO_4$), $HNO_3$, and methane sulfonic acid (MSA), and also includes
196 secondary organic aerosols (SOA). Aerosol size distributions are represented by a sectional aerosol bin approach
197 with four size bins (Georgiou et al., 2018). MOSAIC incorporates the thermodynamic and gas-particle
198 partitioning module described by Zaveri et al.(2008). To reduce the computational cost, we selected a 4-bin
199 MOSAIC mechanism that simulates thermodynamic equilibrium and other aerosol processes such as
200 condensation, coagulation, and nucleation. The same mechanism has been widely used with WRF-Chem for
201 simulations outside India (Bucaram and Bowman, 2021; Sha et al., 2019; Yang et al., 2018), but only a limited
202 number of studies have applied it to the Indian domain to include more detailed chemistry and species (Gupta
203 and Mohan, 2015; Jena et al., 2020; Kumar et al., 2018). The SOA formation in MOSAIC is simulated using the
204 volatility basis set approach (Knote et al., 2015). For consistency with the $PM_{2.5}$ MARGA measurements, we
205 have chosen3-bins according to simulated aerosols size (0.04–0.156 μm; 0.156–0.625 μm; 0.625–2.5 μm) in
206 accordance with the WRF-Chem aerosol size distribution.

207 The model domain covers the entire northern region of India, but here model simulations are compared
208 with the observations at IGIA, New Delhi (28.56° N, 77.09° E). The domain was set with a horizontal grid-
209 spacing of 10 km in both the latitudinal and longitudinal directions. The model top vertical grid included 47
210 vertical levels, with the model top set to 10 hPa. The physical parameterization schemes of model configuration
211 are the same as those described by Ghude et al. (2020) and Jena et al. (2021). EDGAR-HTAP (Emission
212 Database for Global Atmospheric Research for Hemispheric Transport of Air Pollution) for the year 2010 at 0.1°
213 x 0.1° grid resolution was used in this study for anthropogenic emissions of aerosols and trace gases ($PM_{2.5}$,
214 $PM_{10}$, OC, BC, CO, $NO_x$, etc.) and are scaled to 2018 as per Jena et al. (2021). Biogenic emissions are
215 calculated online using the Model of Emissions of Gases and Aerosols from Nature version 2.1 (MEGAN2.1)
216 (Guenther et al., 2006), and dust emissions are based on the traditional Goddard Global Ozone Chemistry
217 Aerosol Radiation and Transport (GOCART) dust scheme that works with MOSAIC (Ginoux et al., 2001). Fire
218 INventory from NCAR (FINNv1.5)was used in this study for daily open biomass burning emissions that are
219 vertically distributed within the model using Freitas et al. (2007). The chemical initial and lateral boundary
220 conditions come from the global model simulations from the Model for Ozone and Related Chemical Tracers
221 (MOZART-4), and the meteorological initial and lateral boundary conditions are provided from the fifth
222 generation European Centre for Medium-Range Weather Forecasts (ECMWF) atmospheric reanalysis of the
223 global climate (ERA5) with six-hourly temporal resolution. The simulations were reinitialized every fifth day to
224 limit the growth of meteorological errors in our simulations, but the chemical fields were carried forward from
225 the previous simulation.

226 **3. Results and Discussion**

227 **3.1 Comparison of temporal variation in $NH_3$, $NH_4^+$, and total $NH_x$ using WRF-Chem and MARGA**

228 **3.1.1 Diurnal variation**

229 To investigate how well a state-of-the-art chemical transport model performs in capturing the diurnal behavior
230 of $NH_3$ and $NH_4^+$, we compared observed and model-simulated diurnal profiles of $NH_3$ and $NH_4^+$. Figure 1

231 displays the comparison of diurnal variation (00:00 to 23:00 Indian Standard Time (IST)) in meteorological
232 parameters (T and RH) at the IGIA site in Delhi (Fig. 1a) along with $NH_3$ and $NH_4^+$ averaged over the study
233 period (Fig. 1b) between observations and model. We adopted diurnal variation in emissions from a recent study
234 by Jena et al. (2021). Note that diurnal variability in the model simulations is primarily controlled by the
235 planetary boundary layer mixing. We first investigated the ability of WRF-Chem to accurately predict the
236 meteorological parameters of RH and T, which are important determinants of the gas-to-aerosol partitioning of
237 (semi-) volatile compounds. As shown in Fig. 1a, simulated T and RH are in reasonable agreement with the
238 observations, with the simulated RH values falling in the range of 50–90 %. Overall, it can be seen that the
239 model shows cold and wet bias compared to the observations but shows warm bias (about 2-3 ℃) and dry bias
240 (about 10-12 %) in the afternoon hours. In spite of the small change in the amplitude of the diurnal cycle of RH,
241 the phase characteristics of the diurnal cycle of both T and RH are reasonably well captured by the model.
242 Figure 1b shows that simulated $NH_3$ and $NH_4^+$ are very different compared with the MARGA measurements.
243 The model predicts an average $NH_3$ and $NH_4^+ \pm 1\sigma$ mass loading of 56.7 ± 14.3 and 14.7 ± 4.9 µg
244 $m^{-3}$ respectively, while MARGA measurements indicate an average $NH_3$ and $NH_4^+ \pm 1\sigma$ mass loading of 28.2 ±
245 12.4 and 36.9 ± 15.1 µg $m^{-3}$, respectively. We find the diurnal variation of gas-phase $NH_3$ is significantly
246 overestimated by the model (Normalised Mean Bias (NMB) = 1.02). On the contrary, $NH_4^+$ is underestimated
247 by about 60 % (NMB = -0.60). Simulated $NH_3$ concentrations peak between 07:00-09:00 and 22:00-23:00 h
248 with bimodal variation, whilst MARGA shows a single peak around 12:00-13:00 h. On the contrary, a nearly
249 flat diurnal profile of $NH_4^+$ is predicted by the model, whereas the average MARGA $NH_4^+$ concentration
250 maxima and minima were observed during night-time (16:00-03:00 h) and daytime (03:00-08:00 and 09:00-
251 16:00 h), respectively.

252 We also looked into the average diurnal profile of $NO_x$ and $NH_3$ during dense fog events, and the
253 details can be found in the supplement (Fig. S1 and S2 in the Supplement). It is evident that the observed
254 daytime peak of $NH_3$ did not coincide with $NO_x$ peaks, suggesting that traffic emissions do not contribute
255 significantly to the observed $NH_3$ rise. The observed correlation between fog water and enhanced $NH_3$ pulses is
256 consistent with what would also be expected from the evaporation of dew (Sutton et al., 1998; Wentworth et al.,
257 2014, 2016) (S2 in the Supplement) but is not sufficient to identify whether it is the main cause of the daytime
258 increase of $NH_3$. In the future, measurements of the dew water $NH_4^+$ and the accumulation of dew water would
259 be ideal for illuminating the contributing processes. The daytime increase in $NH_3$ concentration could be
260 associated with $NH_4^+$ aerosol volatilization driven by an associated sharp change in T and RH (~ 11:00-12:00 h)
261 (Sutton et al., 2009a, 2013) off-ground surfaces. The fastest increase in T is 12:00 h, which is indeed when $NH_3$
262 was at maximum concentration indicating gas-to-particle partitioning may impact the diurnal behavior of $NH_3$ at
263 Delhi during winter (Sutton et al., 2009a, 2009b). However, in the model, because the largest increase in
264 simulated $NH_3$ also precedes the large changes in simulated meteorological parameters, and because the
265 simulated particulate $NH_4^+$ is flat compared to observations, simulated meteorology is ruled out as a significant
266 contribution to high bias in simulated $NH_3$. Also, the current model does not include the bidirectional exchange
267 of $NH_3$ with surfaces such as dew and fog water.

### 3.1.2 Daily mean variation

To assess the validity of the model, the ratio between simulated and observed (model/obs) was tested. Figure 2 displays the model/obs ratio of daily mean variations in the $NH_3$, $NH_4^+$, and total $NH_x$ concentrations. The model shows large differences in $NH_3$ and $NH_4^+$ compared with observations. We find a model/obs higher than 1 (1.5-4.5) in simulated $NH_3$, indicating the model is biased high (NMB = 1.02), while there is a poor agreement for $NH_4^+$ (model/obs less than 0.5), indicating model is biased low (NMB = -0.62). There is good agreement between the modelled total $NH_x$, which is mostly consistent with the observation (model/obs close to 1) with a small bias (NMB = 0.08). Despite the adequate ability of the model to reproduce the accurate total $NH_x$, the model is biased low for $NH_4^+$ and high for $NH_3$, indicating that the model's representation of the gas-to-particle partitioning is not correct. It is, therefore, necessary to understand missing chemical processes in gas-to-particle partitioning responsible for the overestimation of $NH_3$ and underestimation of $NH_4^+$ in the model.

### 3.2 Gas-to-particle partitioning

We investigated the ability of the model to accurately describe the gas-to-particle partitioning of the measurements (MARGA) by evaluating the fraction of total $NH_x$ in the particulate phase ($NH_4^+/NH_x$) (Ellis et al., 2011; Wang et al., 2015) for which statistical values are summarized in Table 1. The correlation coefficient (r) indicates an inverse relationship of $NH_4^+/NH_x$ with $NH_3$ for both MARGA and model (r = -0.57, -0.58, respectively). A strong correlation of the MARGA ratio $NH_4^+/NH_x$ with the dominant anion concentration ($Cl^-$: r = 0.79) was observed. However, the measurement shows a poor relationship between $SO_4^{2-}$ and $NH_4^+/NH_x$ followed by $NO_3^-$, which is probably due to very low concentrations that do not change $NH_4^+/NH_x$ significantly even when $SO_4^{2-}$ and $NO_3^-$ are neutralized (see Fig. 6). By contrast, the model shows a strong correlation between $NH_4^+/NH_x$ with $SO_4^{2-}$ concentration (r = 0.77). MARGA indicates high particulate fractions of $NH_4^+$ and $Cl^-$ while the modeled composition is dominated by $NH_4^+$ and $SO_4^{2-}$. This mismatch is due to the complete absence of $Cl^-$ chemistry in the standard model. The measured $NH_4^+/NH_x$ suggests that anthropogenic HCl may be promoting this increase in particle fraction of $NH_4^+$ and $Cl^-$ via partitioning into the aerosol, deprotonating in the aerosol water, followed by $NH_3$ partitioning and being protonated by the ionization of the strong electrolyte HCl (Chen et al., 2022; Gunthe et al., 2021).

Figure 3 shows the percentage contribution of gases ($NH_3$, $SO_2$, HCl, $HNO_3$, and HONO) and $PM_{2.5}$ aerosol ($NH_4^+$, $SO_4^{2-}$, $NO_3^-$ and $Cl^-$) during the WiFEX measurements. The pie charts for the gases show that $NH_3$ (accounting for 53.3 % of the measured total gas concentration) dominates the gas phase, followed by sulfur dioxide ($SO_2$) (35.61 %), whereas $PM_{2.5}$ aerosol show $NH_4^+$ (49.5 %) as a major cation and $Cl^-$ (29.7 %) as a significant anion followed by $NO_3^-$ (11.7 %) and $SO_4^{2-}$ (9 %). There is also a very high amount of $SO_2$ reaching the site from the nearby industrial area, which is not converted to $SO_4^{2-}$ very quickly (Acharja et al., 2021). In a normally $NH_3$-rich atmosphere, gas-phase oxidation of $SO_2$ is much slower than the aqueous phase oxidation by $O_3$, and due to nearby sources, much of the sulfur is present as $SO_2$ (Li et al., 2007). This appears to be because of the slow rate of gas phase oxidation of $SO_2$. Although the atmosphere is rich in $NH_3$, in principle favoring aqueous phase oxidation via $O_3$, it appears that $O_3$ concentrations are often insufficient (mean = 36.3, median = 33.8, minimum = 26.5, and maximum = 53.9, ug m$^{-3}$ respectively) at the IGIA site (Fig. S3 in the Supplement). Hence for many periods during the WIFEX campaign, $SO_4^{2-}$ and $NO_3^-$ are very low, with the result that the $NH_4^+/NH_x$ ratio does not change appreciably when $SO_4^{2-}$ is neutralized (Table 1).

307        According to thermodynamic equilibrium theory, an aqueous solution maintains charge neutralization

308     initially by balancing $NH_3$ uptake with the uptake of sulfuric acid ($H_2SO_4$) before $HNO_3$ and HCl can partition

309     into the aqueous aerosol; hence all $SO_4^{2-}$ in the condensed phase will be fully neutralized before any $HNO_3$, or

310     HCl can partition (Behera et al., 2013). Typical Delhi winter conditions of excess $NH_3$, high RH, and low T

311     favour gas-to-particle partitioning of $NH_3$. The principal inorganic chemical reactions that occur in aqueous

312     atmospheric aerosols form pairs of non-volatile $NH_4^+$ and acid anions ($SO_4^{2-}$, $NO_3^-$, and $Cl^-$) are summarized in

313     reactions R1 to R3 (Seinfeld et al., 1998).

314     $2NH_{3(g)} + H_2SO_{4(g)} \rightleftarrows NH_4^+ + SO_4^{2-}$                                 (R1)

315     $NH_{3(g)} + HNO_{3(g)} \rightleftarrows NH_4^+ + NO_3^-$                                    (R2)

316     $NH_{3(g)} + HCl_{(g)} \rightleftarrows NH_4^+ + Cl^-$                                        (R3)

317

318     $NH_4^+$ and $Cl^-$ (R3), which are favored by low T and high RH, form a reversible equilibrium with $NH_3$ and HCl

319     (Ianniello et al., 2011; Seinfeld and Pandis, 2016), which was the case during WiFEX. It is likely that high $Cl^-$ in

320     Delhi resulted from gas–to-particle partitioning of HCl into aerosol water in the presence of excess $NH_3$ (R3),

321     with aqueous phase $Cl^-$ stimulating further water uptake and jointly driving aerosol mass composition and

322     growth through co-condensation (Chen et al., 2022; Gunthe et al., 2021). Hence, to understand the driver of the

323     measured $NH_4^+$ and the role of aqueous chemistry, we plotted the fraction of the ratio of HCl to $Cl^-$ (HCl/$Cl^-$) as

324     a function of $NH_4^+$ concentration and RH in Fig. 4. The decrease in the fraction of HCl/$Cl^-$ is associated with an

325     increase in $NH_4^+$ concentration at high RH between 70-100 %. The HCl/$Cl^-$ is highly anticorrelated (r = -0.53)

326     with $NH_4^+$ concentration in the presence of high RH (70-100 %), further supporting the view that HCl promotes

327     the increase in the particle fraction of $NH_4^+$ (49.5 %) with $Cl^-$ (29.7 %) the primary anion.

328         We investigated the directions of local emission sources associated with concentration increases of

329     $NH_3$, $NH_4^+$, $Cl^-$ and $NH_x$ through bivariate polar graphs using the OpenAir software (Carslaw and Ropkins,

330     2012) at the IGIA site. Figure 5 shows the bivariate polar plots of mean $NH_3$ (Fig. 5a), $NH_4^+$ (Fig. 5b), $Cl^-$ (Fig.

331     5c), and total $NH_x$ (Fig. 5d) concentration for the observation period in relation to wind speed and wind

332     direction. The 270-300º sector dominated the wind direction at IGIA (Acharja et al., 2021). Figure 5a shows that

333     the highest $NH_3$ concentration was associated with the winds coming from the east and southeast of the site,

334     where it could have been emitted from dairy farms, including animal houses, yards, and manure storage, as well

335     as by the application to the farmland of urea and other ammoniacal fertilizers, ammoniacal wastes and ruminant

336     urine located at this region (Hindustan Times, 2021; Leytem et al., 2018; Sherlock et al., 1994). Such sources of

337     $NH_3$ volatilization (Hristov et al., 2011; Laubach et al., 2013) can also explain the higher concentrations of total

338     $NH_4^+$ (and, by definition $NH_x$) for air coming from the southeast of the measurement site (Fig. 5b and d). This

339     enhancement in the southeast region is not only affected by emissions but also by meteorology and chemistry.

340     Thus higher $NH_3$ concentration may also bedue to the lack of turbulent mixing, which restricts the dilution of

341     plumes from local point sources at lower wind speeds (Ianniello et al., 2010). The bivariate polar plots of

342     $NH_4^+$ (Fig. 5b) and $Cl^-$ (Fig. 5c) concentration point to the west direction as a principal source for

343     thermodynamic partitioning of $NH_3$ and HCl to the condensed phase to form $NH_4^+$ and $Cl^-$. Two industrial

344     sources are located in this direction: the site is impacted by a cluster in northwest Delhi of industrial processes,

345     such as steel pickling industries, and others include metal finishing and electroplating, which are known to be

346     vital HCl emitters (Acharja et al., 2021; Jaiprakash et al., 2017). Near the source, abundant quantities of $NH_3$

347    may drive the partitioning of HCl to the condensed phase resulting in high concentrations of $NH_4^+$ and $Cl^-$

348    towards the west at lower wind speeds. Thus, high $NH_4^+$ and $Cl^-$ correspond to the lowest $NH_3$ concentration

349    region (inverse relation), which can be observed in Fig. 5a, b, and c, highlighting the importance of nearby HCl

350    industrial sources in driving the particle fraction of $NH_4^+$ and $Cl^-$.

351    To gain insight into the role of $NH_4^+$ in the neutralization of anions ($SO_4^{2-}$, $NO_3^-$ and $Cl^-$), the aerosol

352    neutralization ratio (ANR) was calculated using the observed data. The ANR is defined as the equivalent ratio of

353    $NH_4^+$ to the sum of $SO_4^{2-}$, $NO_3^-$ and $Cl^-$ because these species represent the dominant cations and anions in

354    $PM_{2.5}$, respectively. Figure 6 demonstrates, on average, how well the charge balance works between $Cl^-$, $NO_3^-$

355    and $SO_4^{2-}$ (in µeq $m^{-3}$) as the anions and $NH_4^+$ as the major cation (ANR close to unity), with $Cl^-$ as the most

356    significant anion followed by $NO_3^-$ and $SO_4^{2-}$. The mean $\pm 1\sigma$ ANR value for $PM_{2.5}$ during the observed period

357    was $0.96 \pm 0.14$. It ranges from a minimum of $0.35 \pm 0.04$ to a maximum of $2.31 \pm 0.08$. Higher values than

358    unity may indicate the presence of organic acids in the aerosol, which MARGA does not measure (Acharja et

359    al., 2020). Also, high standard error in Fig.6 indicates the possibility of uncertainties associated with the

360    breakthrough of $NH_3$ spikes on the denuder at high concentration (~ 1 %) (Stieger et al., 2019). However, the

361    good charge balance indicates this wasn't a major issue.There also were certain periods where low

362    concentrations were observed of $Cl^-$ and $NO_3^-$ (03-06 January 2018 and 16-17 January 2018) in Fig.6.

363    Comparing the model/obs for $NH_3$, $NH_4^+$ and total $NH_x$ during these periods provides some degree of validation

364    of the model where sulfur chemistry dominates the reaction with $NH_3$. Figure S4 (in the supplement) shows that

365    model/obs indicates substantial variability which appears to be overestimating $NH_3$ (model/obs>1) while

366    underestimating total $NH_4^+$ (model/obs<1) on average in the model.

**3.3 Influence of HCl/$Cl^-$ chemistry in WRF-Chem**

368    We further conducted three scenario simulations for the period 7-16 January 2018 (10 days) to explore the

369    potential impacts of the addition of anthropogenic chloride (HCl/$Cl^-$) emissions in the concentrations of $NH_3$,

370    $NH_4^+$ and total $NH_x$. We employ the HCl emissions from trash-burning activities in Delhi, as predicted by

371    Sharma et al. (2019) in our model set-up. We tested the three sensitivity experiments named: No HCl (0 mol $km^{-2}$ $h^{-1}$),

372    Base Case HCl ($3\times$ Sharma et al., 2019; 24.8 mol $km^{-2}$ $h^{-1}$), and $3\times$Base HCl (74 mol $km^{-2}$ $h^{-1}$) scenario,

373    reflecting adjustments which are consistent with the more recent upward adjustments in the amount of waste

374    burned in landfills by Chaudhary et al. (2021) and also to reflect additional industrial HCl sources not accounted

375    for in the inventory. Figure 7 presents the box-whiskers plots for secondary inorganic aerosols and trace gases

376    from the observations (MARGA), and those simulated by the model for the three sensitivity experiments. Daily

377    mean $\pm 1\sigma$ values are summarized in Table 2 for three different model scenarios. As can be observed from Fig.

378    7(a-c), increasing the HCl emissions (Fig. 7g) in the model partitions more $NH_3$ to the condensed phase due to

379    its high concentrations, reaching maximum mass loadings of $NH_4^+$ and $Cl^-$ of 70 and 110 µg $m^{-3}$, respectively, in

380    the $3\times$Base HCl scenario, while increasing the total mean $NH_x$ concentration by 15 µg $m^{-3}$ compared to the No

381    HCl run presumably reflecting the longer residence time of $NH_4^+$ for near-surface air measurements.

382    The simulated $NO_3^-$ concentration (Fig. 7e) generally exceeds the measurements in all three

383    experiments; since the main neutralizing species for $NO_3^-$ is $NH_4^+$, it is controlled via the equilibrium between

384    $NO_3^-$, $HNO_{3,}$ and $NH_3$, but also the competition with HCl for free $NH_3$. Simulated $HNO_3$ is significantly

385    underestimated (by ~3 µg $m^{-3}$) (Fig. 7h) by the model compared to the observations. As a consequence, the

386 model suggests that $NO_3^-$ formation from gaseous $NH_3$ and $HNO_3$ cannot occur. The gas fraction of observed

387 $HNO_3$ will be determined by aerosol pH and liquid water content based on $NH_3$ and $NO_3^-$ availability (Nenes et

388 al., 2020). The over-prediction of $NH_3$ concentration in the model compared with the observations generates

389 more $NO_3^-$ (and simultaneously reduces $HNO_3$), with the total fraction of $HNO_3 + NO_3^-$ ($THNO_3$) concentration

390 in the model also exceeding the observed $THNO_3$, which is more strongly affected by reducing the $NH_3$

391 emissions in the model (Fig. S5 in the Supplement). On average, $THNO_3$ reduced by only 0.38 µg m$^{-3}$ in 3×Base

392 HCl compared to the No HCl run. But reducing $NH_3$ emissions by a factor of 3 (-3×$NH_3$_EMI) in the 3×Base

393 HCl scenario reduced mean $THNO_3$ by a further 4.71 µg m$^{-3}$. The extent of partitioning and accumulation of

394 $NH_4NO_3$ depends on T, aerosol water, pH, as well as $NH_3$ availability (Nenes et al., 2020). Our model

395 simulations find that the presence of HCl/Cl$^-$ does not significantly alter $THNO_3$ but that the excess $NH_3$ with

396 missing chloride chemistry is a major contributor and will lead to mismatches in the model between measured

397 simulated gas and particulate matter concentrations.

398 The simulated $SO_4^{2-}$ concentration (Fig. 7f) was underestimated (by ~7.5 µg m$^{-3}$), while gas-phase $SO_2$

399 Fig. 7i) was found to be overestimated by about 16 µg m$^{-3}$ in all three experiments compared with the

400 observations. This may be caused by the fact that the drivers for typical sulfate production via OH or aqueous

401 $H_2O_2$ oxidation pathway are likely to be wrong in the model. The missing chemistry may underly this mismatch

402 and requires further sensitivity studies considering different $SO_2$ oxidation pathways. This requires further

403 study, such as scenario evaluation of altered $SO_2$ emissions in the model, to examine the main pathway(s) for

404 $SO_2$ to $SO_4^{2-}$ conversion. Measurements of OH and other radicals in Delhi are currently lacking, making it

405 difficult to constrain the associated chemical schemes. To investigate the further impact of 3×Base HCl in the

406 model, uptake of gaseous $NH_3$ to form $NH_4^+$ and Cl$^-$ was analyzed via a strong correlation coefficient values of r

407 = 0.84for $NH_4^+/NH_x$ with Cl$^-$ concentration, indicating a fraction of gas-to-particle conversion in the model

408 correlates well with the Cl$^-$ concentration and was reasonably well simulated in the 3×Base HCl run.

409 **3.4 Comparison of the temporal variation in $NH_3$, $NH_4^+$, and $NH_x$ using WRF-Chem (HCl/Cl$^-$) and**
410 **MARGA**

411 **3.4.1 Diurnal variation**

412 Here, diurnal variations of monitored aerosol compounds and gases were analysed to investigate the gas-to-

413 particle conversion of $NH_3$ in the model. We analyzed the simulation results of the3×Base HCl run**.** The diurnal

414 variations for $NH_3$ and $NH_4^+$ are controlled mainly by thermodynamic gas-to-particle partitioning, boundary

415 layer mixing, emission and deposition processes, along with vertical and horizontal advection (Meng et al.,

416 2018). Figure 8 (top) presents the diurnal variations of $NH_3$ and $NH_4^+$ (in µg m$^{-3}$) along with particulate $NH_4^+$,

417 Cl$^-$, $NO_3^-$, $SO_4^2$, $SO_2$, HCl, and $HNO_3$ concentrations (in µeq m$^{-3}$) measured (Fig. 8a (top)) and modeled (Fig. 8b

418 (top)) along with its meteorological parameters such as T and RH (Fig. 8 (bottom)). We adopted diurnal

419 variation in emissions from Jena et al. (2021) based on boundary layer mixing. It can be seen in Fig. 8a (top and

420 bottom) that a much bigger peak in $NH_3$ concentration is observed in the daytime than the modeled (despite

421 turbulence differences), indeed suggesting a much stronger $NH_3$ in the middle of the day (11:00-01:00 h). As

422 evaporation proceeds mainly in the morning (08:00-12:00) getting warmer, the peak is near midday (11:00-

423 13:00 h), rather than in the afternoon (13:00-14:00 h) when warmest, similar to what was also observed in

424 Sutton et al. (1998). Indeed, the decreasing $NH_4^+$ and Cl$^-$ during the late morning (10:00 h) corresponds to the

increasing $NH_3$ peak, which reflects the fact that warming promotes the shift of aerosols to the gas phase. Ammonium decreases more than $NH_3$ during the day, as this also evaporates to form $NH_3$. Similarly, $Cl^-$ evaporates during the day since the HCl concentration increases. However, it can be seen that $NO_3^-$ and $SO_4^{2-}$ are slightly changed diurnally, inferring longer range transport perhaps, whereas HCl and $Cl^-$ are from more local sources. The diurnal variability in gases and aerosols in 3×Base HCl simulations in Fig. 8b (top) is primarily controlled by the planetary boundary layer mixing, meteorology/dispersion, environment (T and RH in Fig. 8b (bottom)), and transport. So presumably, maximum $NH_3$ at 08:00 h is due to limited turbulence/boundary layer, with dilution by mixing after 08:00 h. However, the model is able to represent well the diurnal variation of $NH_4^+$ and $Cl^-$ both in terms of amount and pattern, which was not the case in the No HCl run where $NH_4^+$ was observed to be flat in Section 1. During the hours of 09:00 and 11:00 h, when measured $NH_3$ rises, the model predicts a large decrease in $NH_3$, while during 19:00-23:00 h, when measured $NH_3$ decreases, the model predicts a large increase. Furthermore, the modeled HCl and $HNO_3$ are very low compared to the measurements, whereas $SO_2$ concentration matches well with the observations. It can be seen that $NO_3^-$ and $SO_4^{2-}$ are flat in the model. This highlights the need to develop accurate diurnal variability in $NH_3$ emissions over this region.

Figure 9 presents the differences in diurnal variation of mean $NH_3$ (Fig. 9a), $NH_4^+$ (Fig. 9b), and total $NH_x$ (Fig. 9c) concentration for the three sensitivity experiments. While the simulated $NH_3$ concentrations decrease in the 3×Base HCl compared to the No HCl and Base Case HCl run (Table 2), none of the model experiments capture the diurnal cycle of $NH_3$. Higher levels of observed $NH_3$ during daytime and modeled $NH_3$ during night-time highlight the need to improve diurnal variability in $NH_3$ emissions over this region based on the nature and strength of the actual sources. Between the No HCl and the 3xBase HCl run, the NMB for $NH_3$ reduced from 1.38 to 1.13, and NMB for $NH_4^+$ systematically improved from -0.61 to -0.03. In contrast, NMB for total $NH_x$ increased from 0.12 to 0.39. Table 3 summarizes the statistical indicators for the three sensitivity experiments. An increase in HCl emissions in the 3×Base HCl leads to a higher mass concentration of $NH_4^+$ and $Cl^-$, which also increases total mean $NH_x$ concentration by 22.4 $\mu g \ m^{-3}$, presumably reflecting the longer atmospheric lifetime of $NH_4^+$ compared with $NH_3$. We find consistent high bias in all the simulations for $NH_3$, which is highest during the early morning and at night-time. In order to better understand the relationship between $NH_3$, $NH_4^+$ and $NH_x$ concentrations in the diurnal profile of model, one sensitivity study is conducted in the best case HCl experiment to simulate the response of $NH_x$ concentrations by changing $NH_3$ emissions. In these simulations, only $NH_3$ emissions were reduced further by a factor of 3 (-3×$NH_3$_EMI) in the 3×Base HCl experiment, while all other processes and chemical schemes were unchanged. Figure S6 in the Supplement shows the diel profile of model/obs ratio for $NH_3$ (Fig. S6a), $NH_4^+$ (Fig. S6b), and total $NH_x$ (Fig. S6c) concentration simulated with the 3×Base HCl and -3×$NH_3$_EMI scenario. Reducing $NH_3$ emissions in the model (-3×$NH_3$_EMI) significantly improves model-measurement agreement for $NH_3$ (mean model/obs = 1.9), $NH_4^+$ (mean model/obs = 0.9), and total $NH_x$ concentration(mean model/obs = 1.2) compared to the 3×Base HCl run, further suggesting that the longer lifetime of $NH_4^+$ may be the controlling driver for the total $NH_x$ concentration in the model.

### 3.4.2 Variation of daily means

Figure S7 in the Supplement illustrates a time-series graph that compares daily mean $NH_3$ (Fig.S7a), $NH_4^+$ (Fig. S7b), and total $NH_x$ concentrations (Fig. S7c) for the three sensitivity experiments, and Table 2 shows the mean

464 ± 1σ of these variables. The results show that compared to the No HCl run, $NH_3$ mean concentrations decreased

465 by 2 μg m$^{-3}$ in the Base Case HCl and decreased by a further 3.2 μg m$^{-3}$ in the 3×Base HCl run. On the contrary,

466 $NH_4^+$ mean concentration increases in the Base Case HCl by 7.5 μg m$^{-3}$ and further increases by 13.1 μg m$^{-3}$

467 (3×Base HCl). This decrease in $NH_3$ is associated with the enhanced gas-to-particle conversion of $NH_3$ to $NH_4^+$.

468 Associated with these changes, total mean $NH_x$ also increased by 5.5 and 9.8μg m$^{-3}$ in the Base Case HCl and

469 3×Base HCl, respectively, compared to the No HCl. This is likely due to associated increases in the atmospheric

470 lifetime of $NH_x$ with respect to deposition as the partitioning shifted from the faster depositing gas phase to the

471 aerosol phase. The lifetime of $NH_3$ is very short, a few hours, while that of $NH_4^+$ is 1 to 15 days (Aneja et al.,

472 1998; Nair and Yu, 2020; Pawar et al., 2021; Wang et al., 2020a).

473 To understand further the overestimation of total $NH_x$ in the daily mean variation by the model, we

474 compared 3×Base HCl and -3×NH$_3$_EMI sensitivity experiment. Figure 10 shows the ratio of model/obs for

475 $NH_3$ (Fig. 10a), $NH_4^+$ (Fig. 10b) and total $NH_x$ (Fig. 10c) concentration. It can be seen that the model-

476 measurement agreement improves significantly (model/obs closer to 1) after reducing $NH_3$ emissions for all

477 three metrics. -3×NH$_3$_EMI would reduce the mean $NH_3$, $NH_4^+$, and total $NH_x$ concentration by ~8.1 μg m$^{-3}$,

478 3.2 μg m$^{-3}$, and 11.3 μg m$^{-3}$, respectively, compared to the 3×Base HCl run. Even though reducing $NH_3$

479 emissions, it is still sufficient to react rapidly with the varying HCl in the sensitivity experiments contributing to

480 an increase in $NH_4^+$. As can be seen in Fig. 10b, initially, $NH_4^+$ is somewhat lower, but it increases later and

481 matches the 3×Base HCl run. This suggests that $NH_4^+$ formation in the model is more sensitive to changes in

482 HCl than changes in $NH_3$ emission, while total $NH_x$ agrees well by reducing the $NH_3$ emissions. In general,

483 CTMs have higher $NH_3$ concentration than observations, further supporting models having too much $NH_3$. A

484 few factors might contribute to the model discrepancies for $NH_3$: there are uncertainties in the emission

485 inventory of the bottom-up approach of $NH_3$, and the model does not currently include the bidirectional

486 exchange of $NH_3$ with surfaces, such as dew and fog water. Also, model does not have accurate industrial

487 sources of HCl emission. Diurnal emission profiles are uncertainty for both $NH_3$ and HCl. Furthermore, gas-to-

488 particle partitioning associated with $SO_2$ oxidation pathways in the model is not correct at present.

489 **4. Conclusions**

490 In this study, we have evaluated for the first time in South Asia the performance of a chemical transport model

491 (WRF-Chem) in modeling $NH_3$, $NH_4^+$, and total $NH_x$, by comparing against the WiFEX measurements

492 (MARGA).In daily means, we find $NH_3$ is significantly overestimated by the model, $NH_4^+$ was underestimated

493 while simulated total $NH_x$ agreed well with the measurement, indicating incorrect gas-to-particle partitioning

494 along with missing chemical process may impact this mismatch in the model. The ability of the model to

495 accurately describe the gas-to-particle partitioning of the MARGA was evaluated by the fraction of total $NH_x$(=

496 $NH_3 + NH_4^+$) in the particulate phase ($NH_4^+$/$NH_x$). A strong relation of MARGA $NH_4^+$/$NH_x$ was observed with

497 dominant anion (Cl$^-$) (r = 0.79), whereas the standard model showed a strong correlation between $NH_4^+$/$NH_x$

498 with dominant anion ($SO_4^{2-}$) (r = 0.77), pointing to the missing chloride (HCl/Cl$^-$) chemistry in the model.

499 We incorporated HCl/Cl$^-$ emissions in the model and conducted three sensitivity experiments of varying

500 varying HCl emissions, named as No HCl (0 mol km$^{-2}$ h$^{-1}$), Base Case HCl (3× Sharma et al., 2019; 24.8 mol

501 km$^{-2}$ h$^{-1}$) and 3×Base HCl (74 mol km$^{-2}$ h$^{-1}$) run. The revised model shows that by adding HCl emissions more

502 $NH_x$ was partitioned to the condensed phase improving agreement with the observations.3×Base HCl was able

503    to represent well the diurnal variation of $NH_4^+$ and $Cl^-$ both in terms of amount and pattern with improved NMB

504    for $NH_3$.Additional sensitivities tests in changing $NH_3$ emissions (reduction by a factor of 3) in the 3×Base HCl

505    also improved $NH_3$, $NH_4^+$, and $NH_x$ concentrations. We find excess $NH_3$ along with longer lifetime of $NH_4^+$ may

506    act as a controlling driver for $NH_x$ overestimation in the model. These results highlight the need to include

507    correct industrial sources of HCl emissions along with appropriate emissions of $NH_3$ to reduce biases in $NH_x$.

508    Developing the appropriate $NH_3$ emissions using country-specific emission inventories, which are currently

509    under development as part of the Global Challenges Research Fund (GCRF), South Asian Nitrogen Hub

510    (SANH). Also, there is potential to develop top-down constraints on $NH_3$ emissions by taking inference from

511    the satellite, model, and ground-based observations. Challenges remain in simulating $NH_3$ as a contributor to

512    particulate matter due to temporal factors in ammonia peaks including the role of fog and dew where more work

513    is needed. This work also suggests model improvements to $SO_2$ oxidation pathways could improve $NH_x$

514    partitioning.

515    **Data availability**

516    The $0.1^{°} \times 0.1^{°}$ emission grid maps can be downloaded from the EDGAR website on

517    https://edgar.jrc.ec.europa.eu/htap_v2/index.php?SECURE=_123 per year per sector.Gridded emissions in t $y^{-1}$

518    on a $0.1° \times 0.1°$ for HCl emissions can be downloaded from Mendeley data: http://dx.doi.org/10.

519    17632/546t9249bv.1.The model data is available at Aditya, Indian Institute of Tropical Meteorology

520    (IITM) super-computer and can be provided upon request to the corresponding author.The observational and

521    meteorological data of WiFEX are available by contacting the corresponding author.

522    **Author contributions**

523    SDG designed the research; PVP performed the WRF-Chem model simulations andled the analysis; PA and RK

524    contributed to data collection and its quality control and assurance; GG, RK, and PG helped with the model set

525    up; PVP and SDG wrote the paper with contributions from all co-authors.

526    **Competing interests**

527    The authors declare that they have no conflict of interest.

528    **Acknowledgments**

529    We thank the Director, IITM, for his continuous support and encouragement. IITM is funded by the Ministry of

530    Earth Sciences (MoES), Government of India. We wish to thank the MoES for supporting the WiFEX

531    campaign. The lead author's fellowship was supported by the National Supercomputing Mission (NSM)

532    program grant at C-DAC, and Ph.D. fees are covered by the Natural Environment Research Council (NERC) of

533    UK Research and Innovation (UKRI)-Global Challenges Research Fund (GCRF), South Asian Nitrogen Hub

534    (SANH), and we are grateful to the Executive Director and the Director-General of C-DAC and the SANH

535     Director and Chair of the Executive Board. We acknowledge the availability of CPCB-NO$_x$, NO$_2$, and O$_3$ data

536     from the CPCB web portal (https://app.cpcbccr.com/ccr, last access: 1 December 2021). We wish to

537     acknowledge the National Center for Atmospheric Research is sponsored by the National Science Foundation.

538     **5. References**

539     Acharja, P., Ali, K., Trivedi, D. K., Safai, P. D., Ghude, S., Prabhakaran, T. and Rajeevan, M.: Characterization

540     of atmospheric trace gases and water soluble inorganic chemical ions of PM1 and PM2.5 at Indira Gandhi

541     International Airport, New Delhi during 2017–18 winter, Sci. Total Environ., 729, 138800,

542     doi:10.1016/j.scitotenv.2020.138800, 2020.

543     Acharja, P., Ali, K., Ghude, S. D., Sinha, V., Sinha, B., Kulkarni, R., Gultepe, I. and Nair, M.: Chemosphere

544     Enhanced secondary aerosol formation driven by excess ammonia during fog episodes, Chemosphere,

545     289(November 2021), 133155, doi:10.1016/j.chemosphere.2021.133155, 2021.

546     Ali, K., Acharja, P., Trivedi, D. K., Kulkarni, R., Pithani, P., Safai, P. D., Chate, D. M., Ghude, S., Jenamani, R.

547     K. and Rajeevan, M.: Characterization and source identification of PM 2.5 and its chemical and carbonaceous

548     constituents during Winter Fog Experiment 2015–16 at Indira Gandhi International Airport, Delhi, Sci. Total

549     Environ., 662, 687–696, doi:10.1016/j.scitotenv.2019.01.285, 2019.

550     Aneja, V. P., Murray, G. C. and Southerland, J.: Atmospheric nitrogen compounds: Emissions, transport,

551     transformation, deposition, and assessment, EM Air Waste Manag. Assoc. Mag. Environ. Manag., 22–25, 1998.

552     Behera, S. N., Sharma, M., Aneja, V. P. and Balasubramanian, R.: Ammonia in the atmosphere: a review on

553     emission sources, atmospheric chemistry and deposition on terrestrial bodies, Environ. Sci. Pollut. Res., 20(11),

554     8092–8131, doi:10.1007/s11356-013-2051-9, 2013.

555     Bucaram, C. J. and Bowman, F. M.: Wrf-chem modeling of summertime air pollution in the northern great

556     plains:  Chemistry  and  aerosol  mechanism  intercomparison,  Atmosphere  (Basel).,  12(9),

557     doi:10.3390/atmos12091121, 2021.

558     Carslaw, D. C. and Ropkins, K.: Openair - An r package for air quality data analysis, Environ. Model. Softw.,

559     27–28(July 2019), 52–61, doi:10.1016/j.envsoft.2011.09.008, 2012.

560     Chaudhary, P., Garg, S., George, T., Shabin, M., Saha, S., Subodh, S. and Sinha, B.: Underreporting and open

561     burning – the two largest challenges for sustainable waste management in India, Resour. Conserv. Recycl., 175,

562     105865, doi:https://doi.org/10.1016/j.resconrec.2021.105865, 2021.

563     Chen, Y., Wang, Y., Nenes, A., Wild, O., Song, S., Hu, D., Liu, D., He, J., Hildebrandt Ruiz, L., Apte, J. S.,

564     Gunthe, S. S. and Liu, P.: Ammonium Chloride Associated Aerosol Liquid Water Enhances Haze in Delhi,

565     India, Environ. Sci. Technol., 56(11), 7163–7173, doi:10.1021/acs.est.2c00650, 2022.

566     Clarisse, L., Clerbaux, C., Dentener, F., Hurtmans, D. and Coheur, P. F.: Global ammonia distribution derived

567     from infrared satellite observations, Nat. Geosci., 2(7), 479–483, doi:10.1038/ngeo551, 2009.

568     Clarisse, L., Shephard, M. W., Dentener, F., Hurtmans, D., Cady-Pereira, K., Karagulian, F., Van Damme, M.,

569     Clerbaux, C. and Coheur, P. F.: Satellite monitoring of ammonia: A case study of the San Joaquin Valley, J.

570     Geophys. Res. Atmos., 115(13), 1–15, doi:10.1029/2009JD013291, 2010.

571     CPCB: Annual Report 2014-15., 2014.

572     CPCB: Annual Report Annual Report., 2020.

573     Van Damme, M., Clarisse, L., Whitburn, S., Hadji-Lazaro, J., Hurtmans, D., Clerbaux, C. and Coheur, P. F.:

Industrial and agricultural ammonia point sources exposed, Nature, 564(7734), 99–103, doi:10.1038/s41586-018-0747-1, 2018.

Datta, A., Sharma, S. K., Harit, R. C., Kumar, V., Mandal, T. K. and Pathak, H.: Ammonia emission from subtropical crop land area in india, Asia-Pacific J. Atmos. Sci., 48(3), 275–281, doi:10.1007/s13143-012-0027-1, 2012.

Duan, X., Yan, Y., Peng, L., Xie, K., Hu, D., Li, R. and Wang, C.: Role of ammonia in secondary inorganic aerosols formation at an ammonia-rich city in winter in north China: A comparative study among industry, urban, and rural sites, Environ. Pollut., 291(May), 118151, doi:10.1016/j.envpol.2021.118151, 2021.

Ellis, R. A., Murphy, J. G., Markovic, M. Z., Vandenboer, T. C., Makar, P. A., Brook, J. and Mihele, C.: The influence of gas-particle partitioning and surface-atmosphere exchange on ammonia during BAQS-Met, Atmos. Chem. Phys., 11(1), 133–145, doi:10.5194/acp-11-133-2011, 2011.

FINNv1.5: FINN Data, [online] Available from: http://bai.acom.ucar.edu/Data/fire/ (Accessed 15 April 2019), n.d.

Freitas, S. R., Longo, K. M., Chatfield, R., Latham, D., Silva Dias, M. A. F., Andreae, M. O., Prins, E., Santos, J. C., Gielow, R. and Carvalho Jr., J. A.: Including the sub-grid scale plume rise of vegetation fires in low resolution atmospheric transport models, Atmos. Chem. Phys., 7(13), 3385–3398, doi:10.5194/acp-7-3385-2007, 2007.

Georgiou, G. K., Christoudias, T., Proestos, Y., Kushta, J., Hadjinicolaou, P. and Lelieveld, J.: Air quality modelling in the summer over the eastern Mediterranean using WRF-Chem: chemistry and aerosol mechanism intercomparison, Atmos. Chem. Phys., 18(3), 1555–1571, doi:10.5194/acp-18-1555-2018, 2018.

Ghude, S., Kumar, R., Jena, C., Debnath, S., Kulkarni, R., Alessandrini, S., Biswas, M., Kulkrani, S., Pithani, P., Kelkar, S., Sajjan, V., Chate, D., Soni, V., Singh, S., Nanjundiah, R. and Rajeevan, M.: Evaluation of PM2.5 Forecast using Chemical Data Assimilation in the WRF-Chem Model: A Novel Initiative Under the Ministry of Earth Sciences Air Quality Early Warning System for Delhi, India, Curr. Sci., 118, doi:10.18520/cs/v118/i11/1803-1815, 2020.

Ghude, S. D.: Premature mortality in India due to PM2.5 and ozone exposure, Geophys. Res. Lett., 1–8, doi:10.1002/2013GL058740.Received, 2016.

Ghude, S. D., Fadnavis, S., Beig, G., Polade, S. D. and van der A, R. J.: Detection of surface emission hot spots, trends, and seasonal cycle from satellite-retrieved NO$_2$ over India, J. Geophys. Res., 113(D20), D20305, doi:10.1029/2007JD009615, 2008a.

Ghude, S. D., Jain, S. L., Arya, B. C., Beig, G., Ahammed, Y. N., Kumar, A. and Tyagi, B.: Ozone in ambient air at a tropical megacity, Delhi: Characteristics, trends and cumulative ozone exposure indices, J. Atmos. Chem., 60(3), 237–252, doi:10.1007/s10874-009-9119-4, 2008b.

Ghude, S. D., Van der A, R. J., Beig, G., Fadnavis, S. and Polade, S. D.: Satellite derived trends in NO2 over the major global hotspot regions during the past decade and their inter-comparison, Environ. Pollut., 157(6), 1873–1878, doi:10.1016/j.envpol.2009.01.013, 2009.

Ghude, S. D., Lal, D. M., Beig, G., van der A, R. and Sable, D.: Rain-Induced Soil NO$_x$ Emission From India During the Onset of the Summer Monsoon: A Satellite Perspective, J. Geophys. Res., 115(D16), D16304, doi:10.1029/2009JD013367, 2010.

Ghude, S. D., Pfister, G. G., Jena, C. K., Emmons, L. K., Kumar, R. and van der A, R. J.: Satellite constraints of

Nitrogen Oxide (NOX) emissions from India based on OMI observations and WRF-Chem simulations, Geophys. Res. Lett., 40(x), 423–428, doi:10.1029/2012gl053926, 2012.

Ghude, S. D., Kulkarni, S. H., Jena, C., Pfister, G. G., Beig, G., Fadnavis, S. and Van Der, R. J.: Application of satellite observations for identifying regions of dominant sources of nitrogen oxides over the indian subcontinent, J. Geophys. Res. Atmos., 118(2), 1075–1089, doi:10.1029/2012JD017811, 2013.

Ghude, S. D., Bhat, G. S., Prabhakaran, T., Jenamani, R. K., Chate, D. M., Safai, P. D., Karipot, A. K., Konwar, M., Pithani, P., Sinha, V., Rao, P. S. P., Dixit, S. A., Tiwari, S., Todekar, K., Varpe, S., Srivastava, A. K., Bisht, D. S., Murugavel, P., Ali, K., Mina, U., Dharua, M., Rao, Y. J., Padmakumari, B., Hazra, A., Nigam, N., Shende, U., Lal, D. M., Chandra, B. P., Mishra, A. K., Kumar, A., Hakkim, H., Pawar, H., Acharja, P., Kulkarni, R., Subharthi, C., Balaji, B., Varghese, M., Bera, S. and Rajeevan, M.: Winter fog experiment over the Indo-Gangetic plains of India, Curr. Sci., 112(4), doi:10.18520/cs/v112/i04/767-784, 2017.

Ghude, S. D., Kumar, R., Govardhan, G., Jena, C., Nanjundiah, R. S. and Rajeevan, M.: New Delhi: air-quality warning system cuts peak pollution, Nature, 602(7896), 211, doi:10.1038/D41586-022-00332-Y, 2022.

Ginoux, P., Chin, M., Tegen, I., Goddard, T. and In-, G.: Sources and distribution of dust aerosols simulated with the GOCART model, J. Geophys. Res., 106, 20255–20273, doi:https://doi.org/10.1029/2000JD000053, 2001.

Gu, B., Zhang, L., Dingenen, R. Van, Vieno, M., Grinsven, H. J. Van, Zhang, X., Zhang, S., Chen, Y., Wang, S., Ren, C., Rao, S., Holland, M., Winiwarter, W., Chen, D., Xu, J. and Sutton, M. A.: Abating ammonia is more cost-effective than nitrogen oxides for mitigating PM2.5 air pollution, Science (80-. )., 374(6568), 758–762, doi:10.1126/science.abf8623, 2021.

Guenther, A., Karl, T., Harley, P., Wiedinmyer, C., Palmer, P. I. and Geron, C.: Estimates of global terrestrial isoprene emissions using MEGAN (Model of Emissions of Gases and Aerosols from Nature), Atmos. Chem. Phys., 6(11), 3181–3210, doi:10.5194/acp-6-3181-2006, 2006.

Gunthe, S. S., Liu, P., Panda, U., Raj, S. S., Sharma, A., Darbyshire, E., Reyes-Villegas, E., Allan, J., Chen, Y., Wang, X., Song, S., Pöhlker, M. L., Shi, L., Wang, Y., Kommula, S. M., Liu, T., Ravikrishna, R., McFiggans, G., Mickley, L. J., Martin, S. T., Pöschl, U., Andreae, M. O. and Coe, H.: Enhanced aerosol particle growth sustained by high continental chlorine emission in India, Nat. Geosci., 14(2), 77–84, doi:10.1038/s41561-020-00677-x, 2021.

Gupta, M. and Mohan, M.: Validation of WRF/Chem model and sensitivity of chemical mechanisms to ozone simulation over megacity Delhi, Atmos. Environ., 122, 220–229, doi:10.1016/j.atmosenv.2015.09.039, 2015.

Hindustan Times: 66 dairies, six dyeing units shut down in east Delhi, Hindustan Times, 6th July, 2021.

Hristov, A. N., Hanigan, M., Cole, A., Todd, R., McAllister, T. A., Ndegwa, P. M. and Rotz, A.: Review: Ammonia emissions from dairy farms and beef feedlots, Can. J. Anim. Sci., 91(1), 1–35, doi:10.4141/CJAS10034, 2011.

Huang, X., Song, Y., Li, M., Li, J., Huo, Q., Cai, X., Zhu, T., Hu, M. and Zhang, H.: A high-resolution ammonia emission inventory in China, Global Biogeochem. Cycles, 26(1), 1–14, doi:10.1029/2011GB004161, 2012.

Ianniello, A., Spataro, F., Esposito, G., Allegrini, I., Rantica, E., Ancora, M. P., Hu, M. and Zhu, T.: Occurrence of gas phase ammonia in the area of Beijing (China), Atmos. Chem. Phys., 10(19), 9487–9503, doi:10.5194/acp-10-9487-2010, 2010.

Ianniello, A., Spataro, F., Esposito, G., Allegrini, I., Hu, M. and Zhu, T.: Chemical characteristics of inorganic ammonium salts in PM2.5 in the atmosphere of Beijing (China), Atmos. Chem. Phys., 11(21), 10803–10822, doi:10.5194/acp-11-10803-2011, 2011.

Jaiprakash, Singhai, A., Habib, G., Raman, R. S. and Gupta, T.: Chemical characterization of PM1.0 aerosol in Delhi and source apportionment using positive matrix factorization, Environ. Sci. Pollut. Res., 24(1), 445–462, doi:10.1007/s11356-016-7708-8, 2017.

Jena, C., Ghude, S., Kulkarni, R., Debnath, S., Kumar, R., Soni, V. K., Acharja, P., Kulkarni, S., Khare, M., Kaginalkar, A., Chate, D., Ali, K., Nanjundiah, R. and Rajeevan, M.: Evaluating the sensitivity of fine particulate matter (PM$_{2.5}$) simulations to chemical mechanism in Delhi, Atmos. Chem. Phys. Discuss., (3), 1–28, doi:10.5194/acp-2020-673, 2020.

Jena, C., Ghude, S. D., Kumar, R., Debnath, S., Govardhan, G., Soni, V. K., Kulkarni, S. H., Beig, G., Nanjundiah, R. S. and Rajeevan, M.: Performance of high resolution (400 m) PM2.5 forecast over Delhi, Sci. Rep., 11(1), 1–9, doi:10.1038/s41598-021-83467-8, 2021.

Knote, C., Hodzic, A. and Jimenez, J. L.: The effect of dry and wet deposition of condensable vapors on secondary organic aerosols concentrations over the continental US, Atmos. Chem. Phys., 15(1), 1–18, doi:10.5194/acp-15-1-2015, 2015.

Kulkarni, S. H., Ghude, S. D., Jena, C., Karumuri, R. K., Sinha, B., Sinha, V., Kumar, R., Soni, V. K. and Khare, M.: How Much Does Large-Scale Crop Residue Burning Affect the Air Quality in Delhi?, Environ. Sci. Technol., 54(8), 4790–4799, doi:10.1021/acs.est.0c00329, 2020.

Kumar, A., Hakkim, H., Ghude, S. D. and Sinha, V.: Probing wintertime air pollution sources in the Indo-Gangetic Plain through 52 hydrocarbons measured rarely at Delhi & Mohali, Sci. Total Environ., 801, 149711, doi:https://doi.org/10.1016/j.scitotenv.2021.149711, 2021.

Kumar, R., Barth, M. C., Pfister, G. G., Delle Monache, L., Lamarque, J. F., Archer-Nicholls, S., Tilmes, S., Ghude, S. D., Wiedinmyer, C., Naja, M. and Walters, S.: How Will Air Quality Change in South Asia by 2050?, J. Geophys. Res. Atmos., 123(3), 1840–1864, doi:10.1002/2017JD027357, 2018.

Kumar, R., Ghude, S. D., Biswas, M., Jena, C., Alessandrini, S., Debnath, S., Kulkarni, S., Sperati, S., Soni, V. K., Nanjundiah, R. S. and Rajeevan, M.: Enhancing Accuracy of Air Quality and Temperature Forecasts During Paddy Crop Residue Burning Season in Delhi Via Chemical Data Assimilation, J. Geophys. Res. Atmos., 125(17), 1–16, doi:10.1029/2020JD033019, 2020.

Kuttippurath, J., Singh, A., Dash, S. P., Mallick, N., Clerbaux, C., Van Damme, M., Clarisse, L., Coheur, P. F., Raj, S., Abbhishek, K. and Varikoden, H.: Record high levels of atmospheric ammonia over India: Spatial and temporal analyses, Sci. Total Environ., 740, 139986, doi:10.1016/j.scitotenv.2020.139986, 2020.

Lan, Z., Lin, W., Pu, W. and Ma, Z.: Measurement report: Exploring NH3behavior in urban and suburban Beijing: Comparison and implications, Atmos. Chem. Phys., 21(6), 4561–4573, doi:10.5194/acp-21-4561-2021, 2021.

Laubach, J., Taghizadeh-Toosi, A., Gibbs, S. J., Sherlock, R. R., Kelliher, F. M. and Grover, S. P. P.: Ammonia emissions from cattle urine and dung excreted on pasture, Biogeosciences, 10(1), 327–338, doi:10.5194/bg-10-327-2013, 2013.

Leytem, A. B., Bjorneberg, D. L., Rotz, C. A., Moraes, L. E., Kebreab, E. and Dungan, R. S.: Ammonia emissions from dairy lagoons in the western U.S., Trans. ASABE, 61(3), 1001–1015, doi:10.13031/trans.12646,

694    2018.

695    Li, L., Chen, Z. M., Zhang, Y. H., Zhu, T., Li, S., Li, H. J., Zhu, L. H. and Xu, B. Y.: Heterogeneous oxidation

696    of sulfur dioxide by ozone on the surface of sodium chloride and its mixtures with other components, J.

697    Geophys. Res. Atmos., 112(18), 1–13, doi:10.1029/2006JD008207, 2007.

698    Makkonen, U., Virkkula, A., Mäntykenttä, J., Hakola, H., Keronen, P., Vakkari, V. and Aalto, P. P.: Semi-

699    continuous gas and inorganic aerosol measurements at a Finnish urban site: comparisons with filters, nitrogen in

700    aerosol and gas phases, and aerosol acidity, Atmos. Chem. Phys., 12(12), 5617–5631, doi:10.5194/acp-12-5617-

701    2012, 2012.

702    Mandal, T. K., Saxena, M., Rohtash, Sharma, S. K., Gupta, N. C., Kumar, M. and Saraswati: Characteristics of

703    ambient ammonia over Delhi, India, Meteorol. Atmos. Phys., 124(1–2), 67–82, doi:10.1007/s00703-013-0299-

704    8, 2013.

705    Meng, Z., Xu, X., Lin, W., Ge, B., Xie, Y., Song, B., Jia, S., Zhang, R., Peng, W., Wang, Y., Cheng, H., Yang,

706    W. and Zhao, H.: Role of ambient ammonia in particulate ammonium formation at a rural site in the North

707    China Plain, Atmos. Chem. Phys., 18(1), 167–184, doi:10.5194/acp-18-167-2018, 2018.

708    Metzger, S., Mihalopoulos, N. and Lelieveld, J.: Importance of mineral cations and organics in gas-aerosol

709    partitioning of reactive nitrogen compounds: Case study based on MINOS results, Atmos. Chem. Phys., 6(9),

710    2549–2567, doi:10.5194/acp-6-2549-2006, 2006.

711    Móring, A., Hooda, S., Raghuram, N., Adhya, T. K., Ahmad, A., Bandyopadhyay, S. K., Barsby, T., Beig, G.,

712    Bentley, A. R., Bhatia, A., Dragosits, U., Drewer, J., Foulkes, J., Ghude, S. D., Gupta, R., Jain, N., Kumar, D.,

713    Kumar, R. M., Ladha, J. K., Mandal, P. K., Neeraja, C. N., Pandey, R., Pathak, H., Pawar, P., Pellny, T. K.,

714    Poole, P., Price, A., Rao, D. L. N., Reay, D. S., Singh, N. K., Sinha, S. K., Srivastava, R. K., Shewry, P., Smith,

715    J., Steadman, C. E., Subrahmanyam, D., Surekha, K., Venkatesh, K., Varinderpal-Singh, Uwizeye, A., Vieno,

716    M. and Sutton, M. A.: Nitrogen Challenges and Opportunities for Agricultural and Environmental Science in

717    India, Front. Sustain. Food Syst., 5, 13, doi:10.3389/fsufs.2021.505347, 2021.

718    Nair, A. A. and Yu, F.: Quantification of atmospheric ammonia concentrations: A review of its measurement

719    and modeling, Atmosphere (Basel)., 11(10), doi:10.3390/atmos11101092, 2020.

720    Nenes, A., Pandis, S. N., Weber, R. J. and Russell, A.: Aerosol pH and liquid water content determine when

721    particulate matter is sensitive to ammonia and nitrate availability, Atmos. Chem. Phys., 20(5), 3249–3258,

722    doi:10.5194/acp-20-3249-2020, 2020.

723    NIVDANGE, S., Jena, C. and Pawar, P.: Nationwide CoViD-19 lockdown impact on air quality in India,

724    MAUSAM, 73(1), 115–128, doi:10.54302/mausam.v73i1.1475, 2022.

725    Pawar, P. V., Ghude, S. D., Jena, C., Móring, A., Sutton, M. A., Kulkarni, S., Lal, D. M., Surendran, D., Van

726    Damme, M., Clarisse, L., Coheur, P.-F., Liu, X., Govardhan, G., Xu, W., Jiang, J. and Adhya, T. K.: Analysis of

727    atmospheric ammonia over South and East Asia based on the MOZART-4 model and its comparison with

728    satellite and surface observations, Atmos. Chem. Phys., 21(8), 6389–6409, doi:10.5194/acp-21-6389-2021,

729    2021.

730    Pinder, R. W., Adams, P. J. and Pandis, S. N.: Ammonia Emission Controls as a Cost-Effective Strategy for

731    Reducing Atmospheric Particulate Matter in the Eastern United States, Environ. Sci. Technol., 41(2), 380–386,

732    doi:10.1021/es060379a, 2007.

733    Pinder, R. W., Gilliland, A. B. and Dennis, R. L.: Environmental impact of atmospheric NH3 emissions under

734    present and future conditions in the eastern United States, Geophys. Res. Lett., 35(12),
735    doi:10.1029/2008GL033732, 2008.

736    Pollution, C. and Board, C.: Guidelines for Manual Sampling & Analyses., 2011.

737    Saraswati, George, M. P., Sharma, S. K., Mandal, T. K. and Kotnala, R. K.: Simultaneous Measurements of
738    Ambient NH 3 and Its Relationship with Other Trace Gases, PM 2.5 and Meteorological Parameters over Delhi,
739    India, Mapan - J. Metrol. Soc. India, 34(1), 55–69, doi:10.1007/s12647-018-0286-0, 2019.

740    Seinfeld, J. H. and Pandis, S. N.: Atmospheric chemistry and physics : from air pollution to climate change., n.d.

741    Seinfeld, J. H., Bretherton, C., Carslaw, K. S., Coe, H., DeMott, P. J., Dunlea, E. J., Feingold, G., Ghan, S.,
742    Guenther, A. B., Kahn, R., Kraucunas, I., Kreidenweis, S. M., Molina, M. J., Nenes, A., Penner, J. E., Prather,
743    K. A., Ramanathan, V., Ramaswamy, V., Rasch, P. J., Ravishankara, A. R., Rosenfeld, D., Stephens, G. and
744    Wood, R.: Improving our fundamental understanding of the role of aerosol–cloud interactions in the climate
745    system, Proc. Natl. Acad. Sci. U. S. A., 113(21), 5781, 2016.

746    Sha, T., Ma, X., Jia, H., Tian, R., Chang, Y., Cao, F. and Zhang, Y.: Aerosol chemical component: Simulations
747    with WRF-Chem and comparison with observations in Nanjing, Atmos. Environ., 218(June), 116982,
748    doi:10.1016/j.atmosenv.2019.116982, 2019.

749    Sharma, C., Tiwari, M. K. and Pathak, H.: Estimates of emission and deposition of reactive nitrogenous species
750    for India, Curr. Sci., 94(11), 1439–1446, 2008.

751    Sharma, G., Sinha, B., Pallavi, Hakkim, H., Chandra, B. P., Kumar, A. and Sinha, V.: Gridded Emissions of
752    CO, NOx, SO2, CO2, NH3, HCl, CH4, PM2.5, PM10, BC, and NMVOC from Open Municipal Waste Burning
753    in India, Environ. Sci. Technol., 53(9), 4765–4774, doi:10.1021/acs.est.8b07076, 2019.

754    Sharma, S. K., Saxena, M., Saud, T., Korpole, S. and Mandal, T. K.: Measurement of NH3, NO, NO2 and
755    related particulates at urban sites of indo gangetic plain (IGP) of India, J. Sci. Ind. Res. (India)., 71(5), 360–362,
756    2012.

757    Sharma, S. K., Harit, R. C., Kumar, V., Mandal, T. K. and Pathak, H.: Ammonia Emission from Rice-Wheat
758    Cropping System in Subtropical Soil of India, Agric. Res., 3(2), 175–180, doi:10.1007/s40003-014-0107-9,
759    2014a.

760    Sharma, S. K., Kumar, M., Rohtash, Gupta, N. C., Saraswati, Saxena, M. and Mandal, T. K.: Characteristics of
761    ambient ammonia over Delhi, India., 2014b.

762    Sharma, S. K., Kotnala, G. and Mandal, T. K.: Spatial Variability and Sources of Atmospheric Ammonia in
763    India: A Review, Aerosol Sci. Eng., 4(1), doi:10.1007/s41810-019-00052-3, 2020.

764    Sherlock, R. R., Freney, J. R., Bacon, P. E. and van der Weerden, T. J.: Estimating ammonia volatilization from
765    unsaturated urea fertilized and urine affected soils by an indirect method, Fertil. Res., 40(3), 197–205,
766    doi:10.1007/BF00750466, 1994.

767    Singh, G. K., Rajeev, P., Paul, D. and Gupta, T.: Chemical characterization and stable nitrogen isotope
768    composition of nitrogenous  component of ambient aerosols from Kanpur in the Indo-Gangetic Plains., Sci.
769    Total Environ., 763, 143032, doi:10.1016/j.scitotenv.2020.143032, 2021.

770    Stieger, B., Spindler, G., van Pinxteren, D., Grüner, A., Wallasch, M. and Herrmann, H.: Development of an
771    online-coupled MARGA upgrade for the 2\,h interval quantification of low-molecular-weight organic acids in
772    the gas and particle phases, Atmos. Meas. Tech., 12(1), 281–298, doi:10.5194/amt-12-281-2019, 2019.

773    Sutton, M. A. and Howard, C. M.: Ammonia maps make history, Nature, 564(7734), 49–50, 2018.

774  Sutton, M. A., Burkhardt, J. K., Guerin, D., Nemitz, E. and Fowler, D.: Development of resistance models to

775  describe measurements of bi-directional ammonia surface-atmosphere exchange, Atmos. Environ., 32(3), 473–

776  480, doi:10.1016/S1352-2310(97)00164-7, 1998.

777  Sutton, M. A., Erisman, J. W., Dentener, F. and Möller, D.: Ammonia in the environment: From ancient times to

778  the present, Environ. Pollut., 156(3), 583–604, doi:10.1016/j.envpol.2008.03.013, 2008.

779  Sutton, M. A., Reis, S. and Baker, S. M. H.: Atmospheric Ammonia: Detecting emission changes and

780  environmental impacts., 2009a.

781  Sutton, M. A., Nemitz, E., Milford, C., Campbell, C., Erisman, J. W., Hensen, A., Cellier, P., David, M.,

782  Loubet, B., Personne, E., Schjoerring, J. K., Mattsson, M., Dorsey, J. R., Gallagher, M. W., Horvath, L.,

783  Weidinger, T., Meszaros, R., Dämmgen, U., Neftel, A., Herrmann, B., Lehman, B. E., Flechard, C. and

784  Burkhardt, J.: Dynamics of ammonia exchange with cut grassland: synthesis of results and conclusions of the

785  GRAMINAE Integrated Experiment, Biogeosciences, 6(12), 2907–2934, doi:10.5194/bg-6-2907-2009, 2009b.

786  Sutton, M. A., Reis, S., Riddick, S. N., Dragosits, U., Nemitz, E., Theobald, M. R., Tang, Y. S., Braban, C. F.,

787  Vieno, M., Dore, A. J., Mitchell, R. F., Wanless, S., Daunt, F., Fowler, D., Blackall, T. D., Milford, C.,

788  Flechard, C. R., Loubet, B., Massad, R., Cellier, P., Personne, E., Coheur, P. F., Clarisse, L., Van Damme, M.,

789  Ngadi, Y., Clerbaux, C., Skjøth, C. A., Geels, C., Hertel, O., Kruit, R. J. W., Pinder, R. W., Bash, J. O., Walker,

790  J. T., Simpson, D., Horváth, L., Misselbrook, T. H., Bleeker, A., Dentener, F. and de Vries, W.: Towards a

791  climate-dependent paradigm of ammonia emission and deposition, Philos. Trans. R. Soc. B Biol. Sci.,

792  368(1621), 20130166–20130166, doi:10.1098/rstb.2013.0166, 2013.

793  Sutton, M. A., Drewer, J., Moring, A., Adhya, T. K., Ahmed, A., Bhatia, A., Brownlie, W., Dragosits, U.,

794  Ghude, S. D., Hillier, J., Hooda, S., Howard, C. M., Jain, N., Kumar, D., Kumar, R. M., Nayak, D. R., Neeraja,

795  C. N., Prasanna, R., Price, A., Ramakrishnan, B., Reay, D. S., Singh, R., Skiba, U., Smith, J. U., Sohi, S.,

796  Subrahmanyan, D., Surekha, K., van Grinsven, H. J. M., Vieno, M., Voleti, S. R., Pathak, H. and Raghuram, N.:

797  2 - The Indian Nitrogen Challenge in a Global Perspective, in The Indian Nitrogen Assessment, edited by Y. P.

798  Abrol, T. K. Adhya, V. P. Aneja, N. Raghuram, H. Pathak, U. Kulshrestha, C. Sharma, and B. Singh, pp. 9–28,

799  Elsevier., 2017a.

800  Sutton, M. A., J. Drewer, A. Moring, T.K Adhya, A. Ahmed and A. Bhatia: The Indian nitrogen assessment :

801  sources of reactive nitrogen, environmental and climate effects, management options, and policies, in The

802  Indian Nitrogen Assessment, edited by Y. P. Abrol, T. K. Adhya, V. P. Aneja, N. Raghuram, H. Pathak, U.

803  Kulshrestha, C. Sharma, and B. Singh, pp. 9–25, Elsevier., 2017b.

804  Sutton, M. A., Van Dijk, N., Levy, P. E., Jones, M. R., Leith, I. D., Sheppard, L. J., Leeson, S., Sim Tang, Y.,

805  Stephens, A., Braban, C. F., Dragosits, U., Howard, C. M., Vieno, M., Fowler, D., Corbett, P., Naikoo, M. I.,

806  Munzi, S., Ellis, C. J., Chatterjee, S., Steadman, C. E., Móring, A. and Wolseley, P. A.: Alkaline air: changing

807  perspectives on nitrogen and air pollution in an ammonia-rich world: Alkaline Air, Philos. Trans. R. Soc. A

808  Math. Phys. Eng. Sci., 378(2183), doi:10.1098/rsta.2019.0315, 2020.

809  Technical specifications for CAAQM station: TECHNICAL SPECIFICATIONS FOR CONTINUOUS

810  AMBIENT AIR QUALITY MONITORING ( CAAQM ) STATION ( REAL TIME ) Central Pollution Control

811  Board East Arjun Nagar , Shahdara., 2019.

812  Thomas, R. M., Trebs, I., Otjes, R., Jongejan, P. A. C., Brink, H. ten, Phillips, G., Kortner, M., Meixner, F. X.

813  and Nemitz, E.: An Automated Analyzer to Measure Surface-Atmosphere Exchange Fluxes of Water Soluble

814    Inorganic Aerosol Compounds and Reactive Trace Gases, Environ. Sci. \& Technol., 43(5), 1412–1418,
815    doi:10.1021/es8019403, 2009.

816    Twigg, M. M., Di Marco, C. F., Leeson, S., van Dijk, N., Jones, M. R., Leith, I. D., Morrison, E., Coyle, M.,
817    Proost, R., Peeters, A. N. M., Lemon, E., Frelink, T., Braban, C. F., Nemitz, E. and Cape, J. N.: Water soluble
818    aerosols and gases at a UK background site – Part 1: Controls of PM$_{2.5}$ and PM$_{10}$ aerosol
819    composition, Atmos. Chem. Phys., 15(14), 8131–8145, doi:10.5194/acp-15-8131-2015, 2015.

820    Wagh, S., Singh, P., Ghude, S. D., Safai, P., Prabhakaran, T. and Kumar, P. P.: Study of ice nucleating particles
821    in fog-haze weather at New Delhi, India: A case of polluted environment, Atmos. Res., 259, 105693,
822    doi:https://doi.org/10.1016/j.atmosres.2021.105693, 2021.

823    Wang, Q., Miao, Y. and Wang, L.: Regional transport increases ammonia concentration in Beijing, China,
824    Atmosphere (Basel)., 11(6), doi:10.3390/ATMOS11060563, 2020a.

825    Wang, S., Nan, J., Shi, C., Fu, Q., Gao, S., Wang, D., Cui, H., Saiz-Lopez, A. and Zhou, B.: Atmospheric
826    ammonia and its impacts on regional air quality over the megacity of Shanghai, China, Sci. Rep., 5(October), 1–
827    13, doi:10.1038/srep15842, 2015.

828    Wang, T., Song, Y., Xu, Z., Liu, M., Xu, T., Liao, W., Yin, L., Cai, X., Kang, L., Zhang, H. and Zhu, T.: Why is
829    the Indo-Gangetic Plain the region with the largest NH3column in the globe during pre-monsoon and monsoon
830    seasons?, Atmos. Chem. Phys., 20(14), 8727–8736, doi:10.5194/acp-20-8727-2020, 2020b.

831    Warner, J. X., Dickerson, R. R., Wei, Z., Strow, L. L., Wang, Y. and Liang, Q.: Increased atmospheric ammonia
832    over the world's major agricultural areas detected from space, Geophys. Res. Lett., 44(6), 2875–2884,
833    doi:10.1002/2016GL072305, 2017.

834    Wentworth, G. R., Murphy, J. G., Gregoire, P. K., Cheyne, C. A. L., Tevlin, A. G. and Hems, R.: Soil-
835    atmosphere exchange of ammonia in a non-fertilized grassland: Measured emission potentials and inferred
836    fluxes, Biogeosciences, 11(20), 5675–5686, doi:10.5194/bg-11-5675-2014, 2014.

837    Wentworth, G. R., Murphy, J. G., Benedict, K. B., Bangs, E. J. and Collett, J. L.: The role of dew as a night-
838    time reservoir and morning source for atmospheric ammonia, Atmos. Chem. Phys., 16(11), 7435–7449,
839    doi:10.5194/acp-16-7435-2016, 2016.

840    Xu, J., Chen, J., Huo, J., Lin, Y., Fu, Q., Guo, H. and Lee, S. H.: Importance of gas-particle partitioning of
841    ammonia in haze formation in the rural agricultural environment, Atmos. Chem. Phys., 20(12), 7259–7269,
842    doi:10.5194/acp-20-7259-2020, 2020.

843    Yang, J., Kang, S. and Ji, Z.: Sensitivity analysis of chemical mechanisms in the WRF-chem model in
844    reconstructing aerosol concentrations and optical properties in the Tibetan Plateau, Aerosol Air Qual. Res.,
845    18(2), 505–521, doi:10.4209/aaqr.2017.05.0156, 2018.

846    Zhang, X., Liu, J., Han, H., Zhang, Y., Jiang, Z., Wang, H., Meng, L., Li, Y. C. and Liu, Y.: Satellite-Observed
847    Variations and Trends in Carbon Monoxide over Asia and Their Sensitivities to Biomass Burning, Remote
848    Sens., 12(5), 830, doi:10.3390/rs12050830, 2020.

849

850

851

852

853

854 **FIGURE CAPTIONS**

855 **Figure 1. Comparison of observed and simulated average diurnal variation in (a) meteorological**

856 **parameters such as Temperature (T in °c) and Relative humidity (RH in %) and (b) $NH_3$ and $NH_4^+$**

857 **concentration (µg m$^{-3}$) during the sampling period (bar indicates mean standard deviation of each hour).**

858

859 **Figure 2. Ratio of model/obs of the daily mean $NH_3$, $NH_4^+$ and total $NH_x$ concentration**

860

861 **Figure 3. Share of major components of gases and particulate matter ($PM_{2.5}$) based on the mean**

862 **concentrations during WiFEX (share according to µeq m$^{-3}$).**

863

864 **Figure 4. Fraction of HCl/Cl$^-$ratio as a function of $NH_4^+$concentration (µgm$^{-3}$) and Relative humidity (RH)**

865

866 **Figure 5. Bivariate plots of mean (a) $NH_3$ concentration (b) $NH_4^+$ concentration (c) Cl$^-$ concentration and**

867 **(d) total $NH_x$ concentration in relation to wind speed (m s$^{-1}$) and direction.**

868

869 **Figure 6. Neutralizing effect between Cl$^-$, $NO_3^-$ and $SO_4^{2-}$ as the anions (µeq m$^{-3}$) and aerosol**

870 **neutralization ratio (ANR) where, ANR>1 indicates over neutralized (alkaline) and ANR<1 indicates**

871 **under neutralized (acid) (orange bar indicates daily mean standard error).**

872

873 **Figure 7. Box-Whiskers plot for trace gases and secondary inorganic aerosols from the observations**

874 **(MARGA) and simulated in sensitivity test with changes in HCl emissions (No HCl (0 mol km$^{-2}$ h$^{-1}$), Base**

875 **Case HCl (24.8 mol km$^{-2}$ h$^{-1}$), and 3×Base HCl (74 mol km$^{-2}$ h$^{-1}$)) at IGIA, Delhi.**

876

877 **Figure 8. (top) Average diurnal cycles of $NH_3$ and $NH_4^+$ concentration(µg m$^{-3}$) with mole equivalents of**

878 **Cl$^-$, $NO_3^-$, $SO_4^{2-}$, $NH_4^+$, $SO_2$, HCl and $HNO_3$ (µeq m$^{-3}$) of (a) measured (MARGA) and (b) modeled (3×Base**

879 **HCl run) along with its meteorological parameters (bottom).**

880

881 **Figure 9. Diurnal variation in the mean (a) $NH_3$ concentration (b) $NH_4^+$ concentration and (c) total $NH_x$**

882 **concentration observed (black), simulated in No HCl (red dotted), Base Case HCl (red dash) and 3×Base**

883 **HCl run (red solid).**

884

885 **Figure 10. Comparison of ratio of model/obs in the daily mean (a) $NH_3$ concentration (b) $NH_4^+$**

886 **concentration and (c) total $NH_x$ concentration in 3×Base HCl and-3×$NH_3$_EMI scenario.**

887

888

889

890

891

892

893

894 **TABLES**

895 **Table 1. Performance statistics of correlation coefficient ($r$) of $NH_4^+/NH_x$ with $NH_3$ and aerosols ($NH_4^+$, $Cl^-$**
896 **, $SO_4^{2-}$, and $NO_3^-$)**

897

| Gases and Aerosols | MARGA Correlation coefficient($r$)with $NH_4^+/NH_x$ ratio | Model Correlation coefficient ($r$) with $NH_4^+/NH_x$ ratio |
|---|---|---|
| Ammonia ($NH_3$) | -0.57 | -0.58 |
| Ammonium ($NH_4^+$) | 0.70 | 0.67 |
| Chloride ($Cl^-$) | 0.79 | - |
| Sulfate ($SO_4^-$) | 0.09 | 0.77 |
| Nitrate ($NO_3^-$) | 0.13 | 0.57 |

898
899
900
901
902
903
904
905
906
907
908
909
910
911
912
913
914
915
916
917
918
919
920
921
922

**Table 2. Daily mean ± 1σ in gases and inorganic aerosol concentration observed (MARGA) and simulated in sensitivity test with changes in total HCl emissions (No HCl (0 mol km$^{-2}$ h$^{-1}$), Base Case HCl (24.8 mol km$^{-2}$ h$^{-1}$), and 3×Base HCl (74 mol km$^{-2}$ h$^{-1}$).**

| Species concentration (μg m$^{-3}$) | MARGA | No HCl | Base Case HCl | 3×Base HCl |
|---|---|---|---|---|
| $NH_3$ | 20 ± 8.52 | 50.2 ± 11.7 | 48.2 ± 11.31 | 44.5 ± 10.8 |
| $NH_4^+$ | 35.9 ± 17.7 | 13.9 ± 3.04 | 21.4 ± 6.65 | 34.5 ± 15.2 |
| $NH_x$ | 56.6 ± 17.1 | 64 ± 13.2 | 69.6 ± 16.6 | 79.5 ± 23.7 |
| $Cl^-$ | 50.6 ± 39.4 | - | 15.1 ± 9.65 | 40.9 ± 27.2 |
| $NO_3^-$ | 27.9 ± 8.17 | 35.9 ± 7.23 | 35.6 ± 7.05 | 35.5 ± 7.03 |
| $SO_4^{2-}$ | 17.1 ± 5.63 | 9.62 ± 2.78 | 9.56 ± 2.71 | 9.56 ± 2.71 |
| HCl | 0.86 ± 0.35 | - | 0.20 ± 0.23 | 0.22 ± 0.25 |
| $HNO_3$ | 3.43 ± 1.68 | 0.18 ± 0.21 | 0.17 ± 0.22 | 0.18 ± 0.23 |
| $SO_2$ | 30.6 ± 18.4 | 46.6 ± 12.4 | 46.7 ± 12.4 | 46.7 ± 12.4 |

**Table 3. Model performance statistics for $NH_3$, $NH_4^+$ and total $NH_x$ concentration at IGIA, Delhi from three sensitivity experiments (No HCl (0 mol km$^{-2}$ h$^{-1}$), Base Case HCl (24.8 mol km$^{-2}$ h$^{-1}$), and 3×Base HCl (74 mol km$^{-2}$ h$^{-1}$)) and the MARGA**

| Species | No HCl | | Base Case HCl | | 3×Base HCl | |
|---|---|---|---|---|---|---|
| | Correlation coefficient ($r$) | Normalised Mean Bias (NMB) | Correlation coefficient ($r$) | Normalised Mean Bias (NMB) | Correlation coefficient ($r$) | Normalised Mean Bias (NMB) |
| $NH_3$ | -0.58 | 1.38 | -0.60 | 1.29 | -0.65 | 1.13 |
| $NH_4^+$ | 0.45 | -0.61 | 0.75 | -0.40 | 0.76 | -0.03 |
| $NH_x$ | 0.69 | 0.12 | 0.70 | 0.22 | 0.70 | 0.39 |

962    **Figure 1**
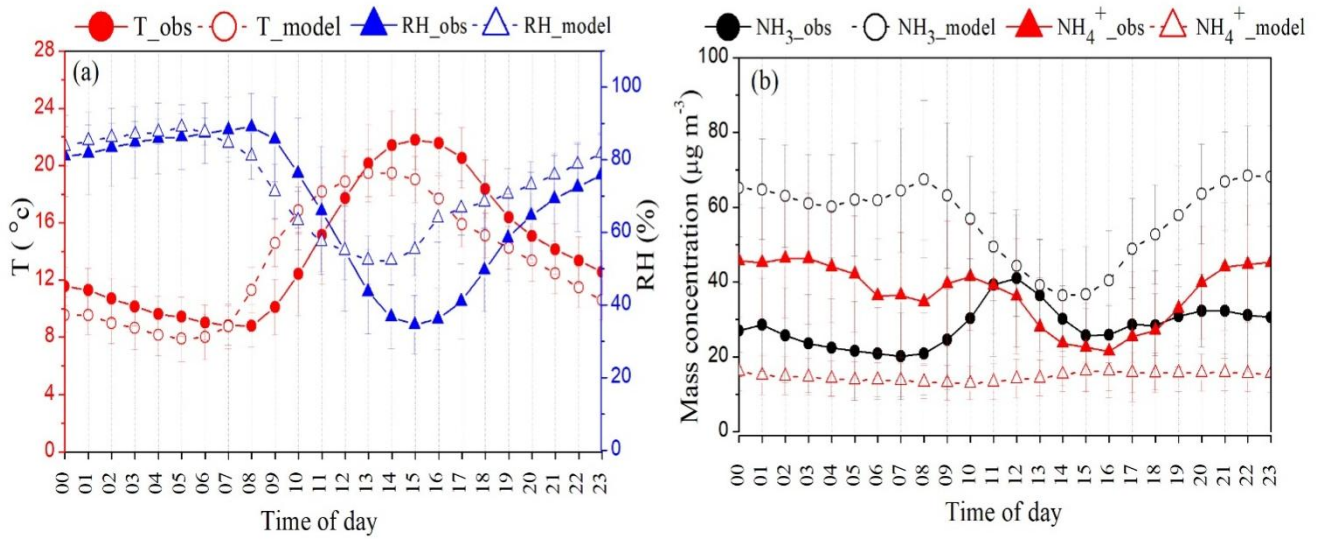
963
964

965    **Figure 2**
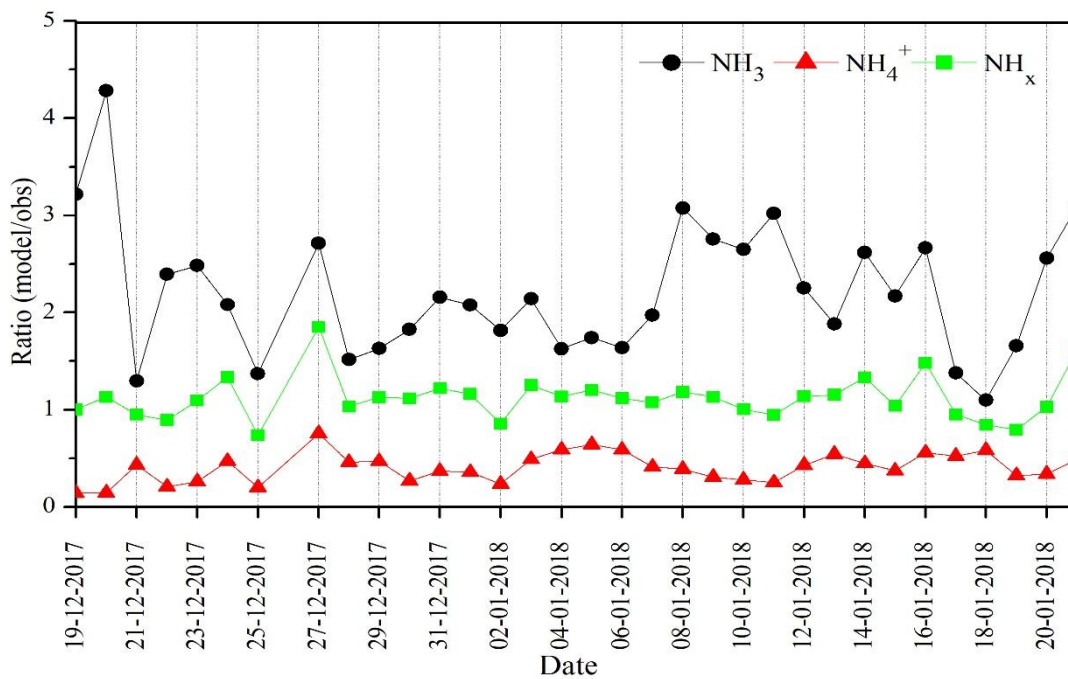
966
967
968
969

970    **Figure 3**
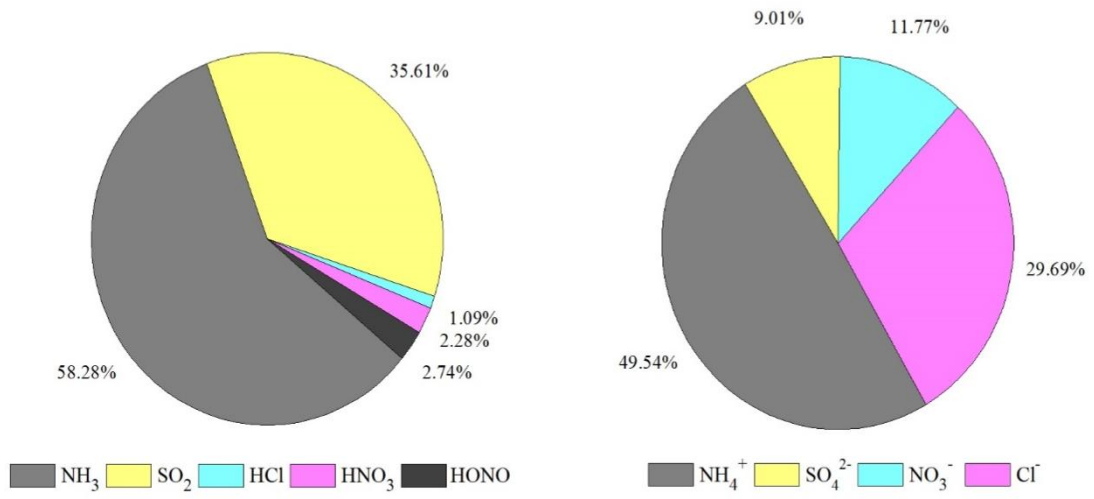
971
972
973

974    **Figure 4**
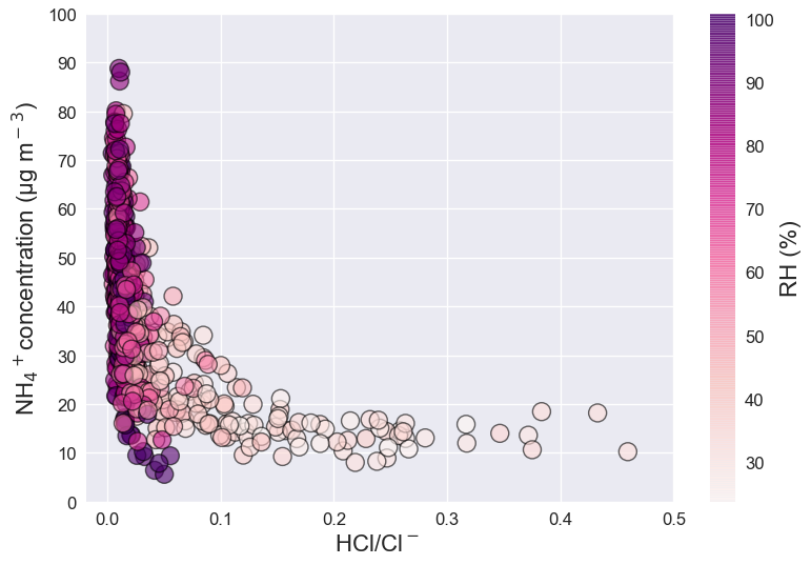
975
976

977

978
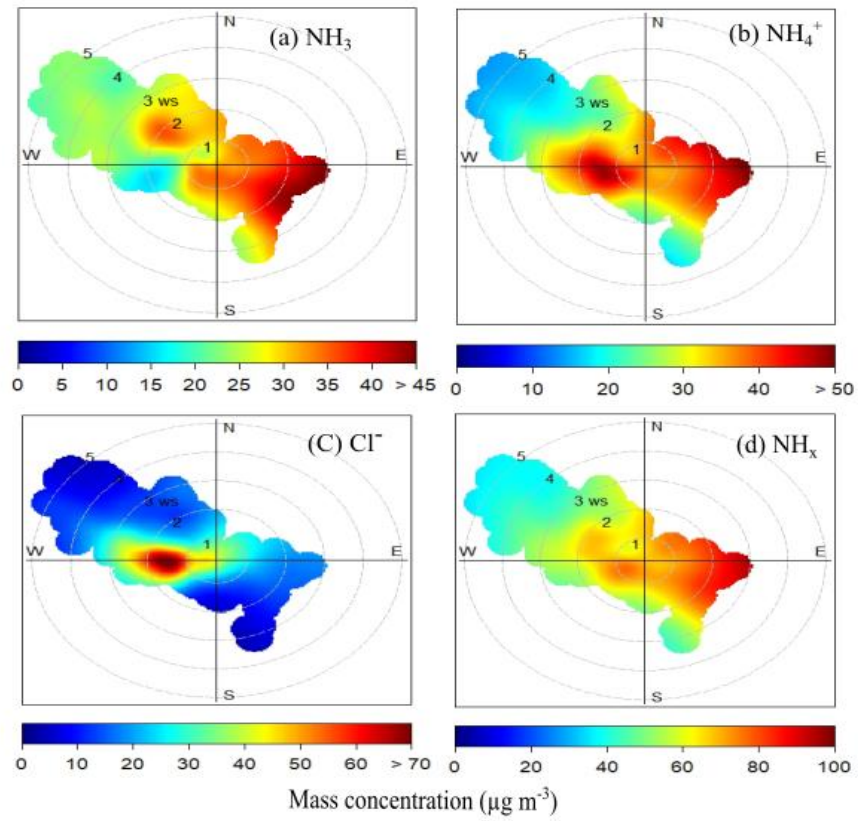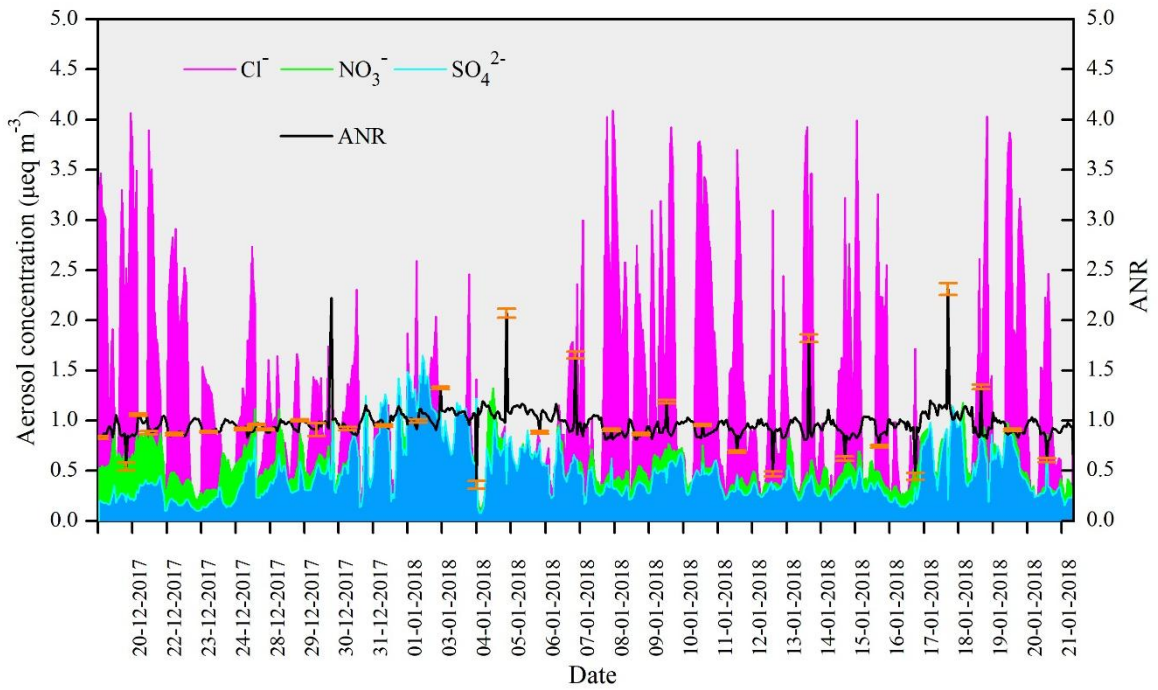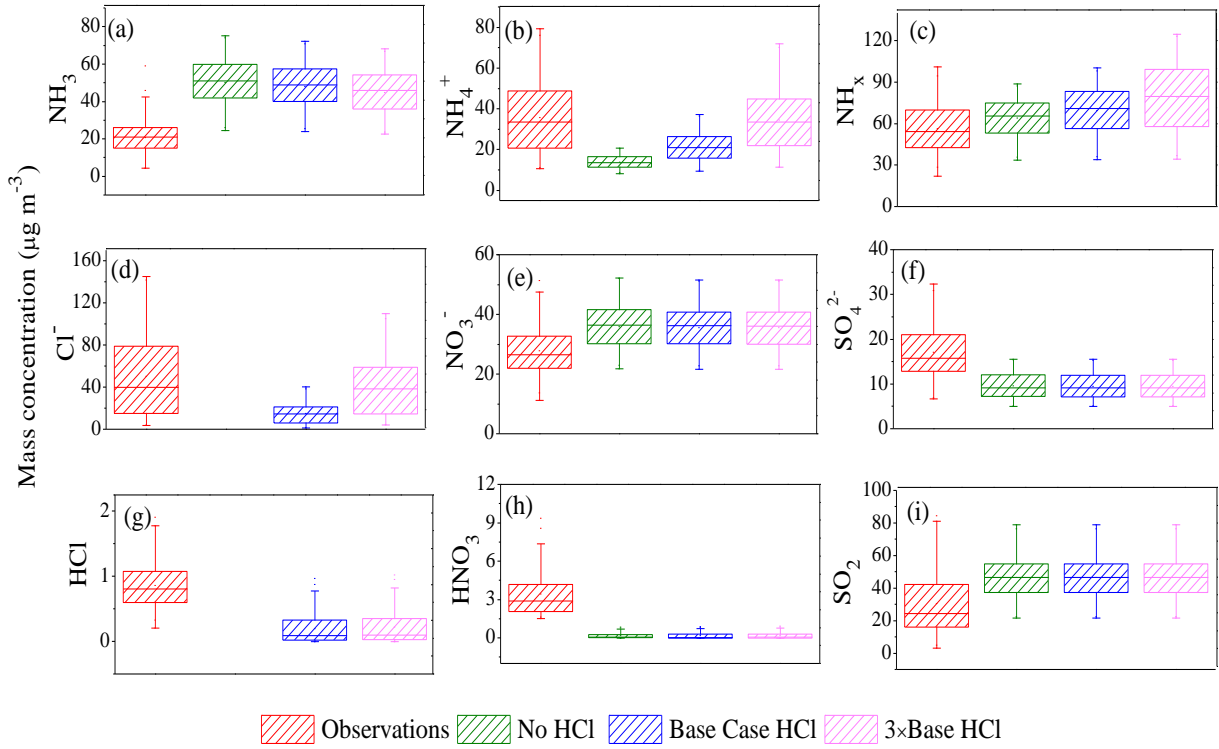
 **Figure 5**

 **Figure 6**

983    **Figure 7**

1003    **Figure 8**
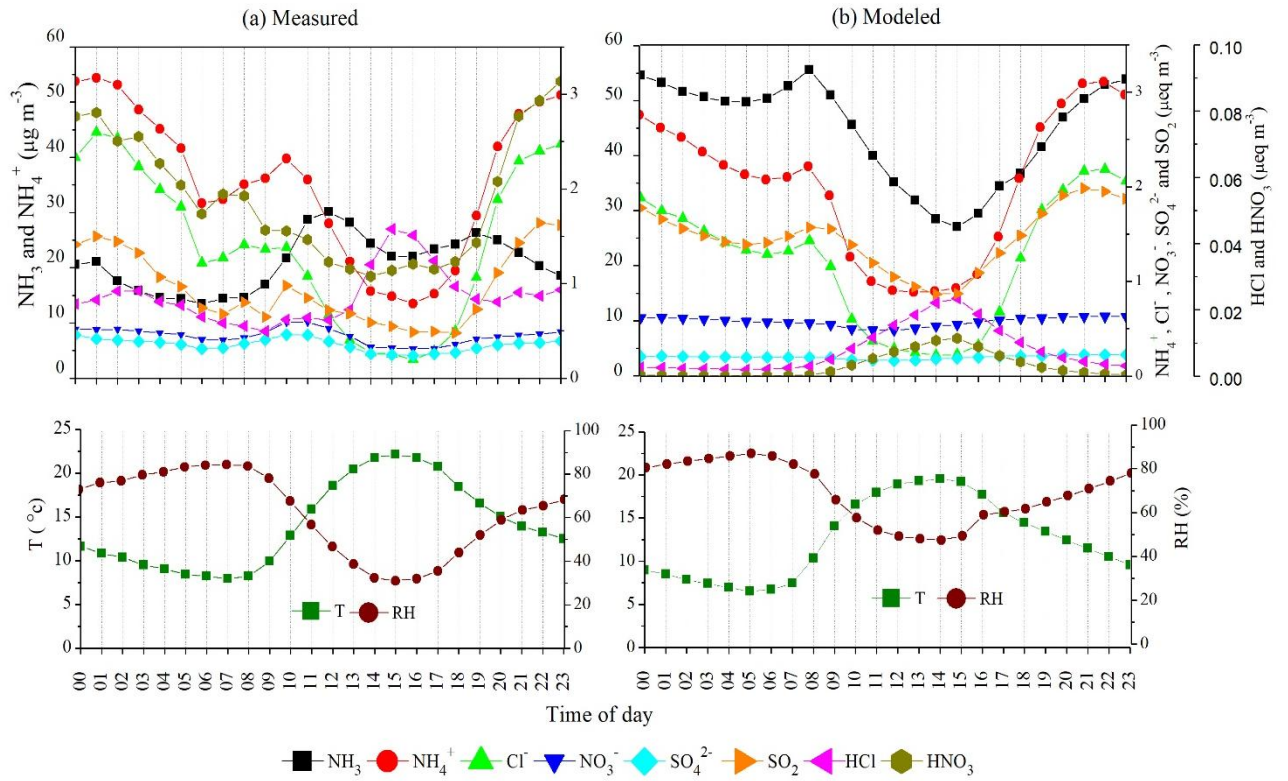
1004
1005
1006
1007
1008
1009
1010
1011
1012
1013
1014
1015
1016
1017
1018
1019
1020
1021
1022

1023  **Figure 9**
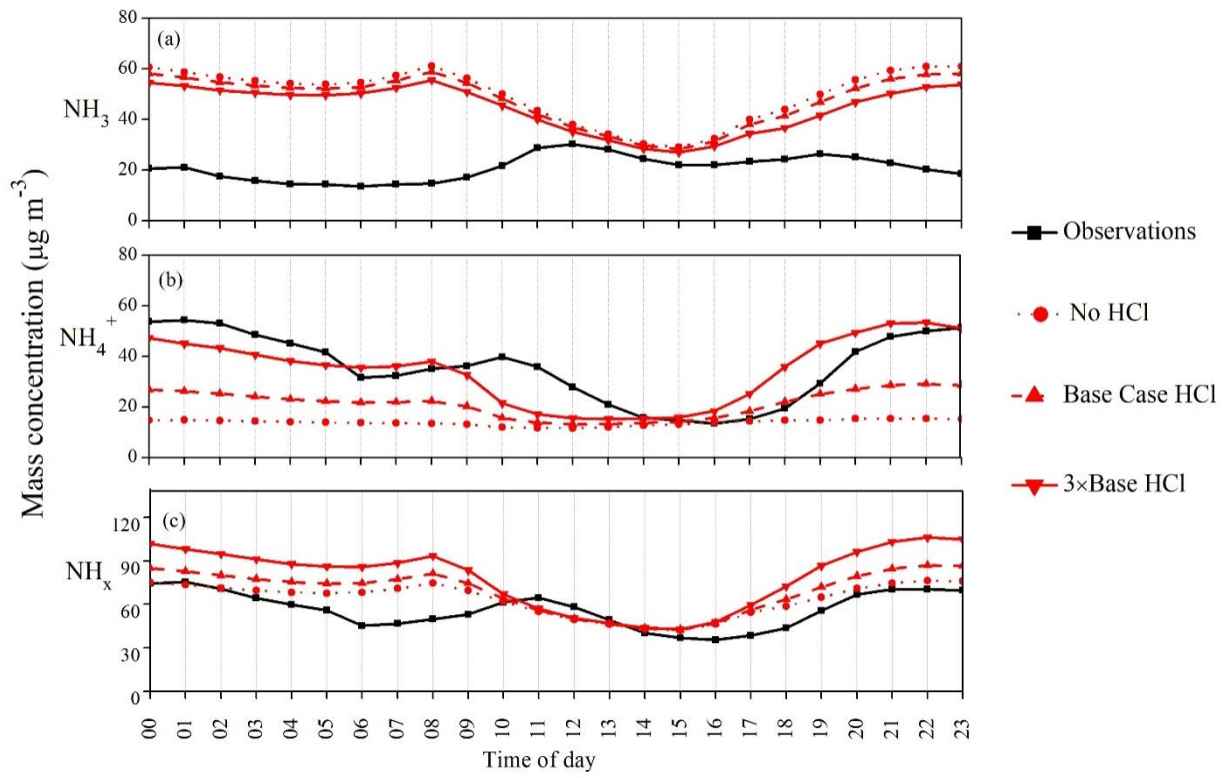
1024

1025

1026

1027

1028

1029

1030

1031

1032

1033

1034

1035

1036

1037

1038

1039

1040 **Figure 10**
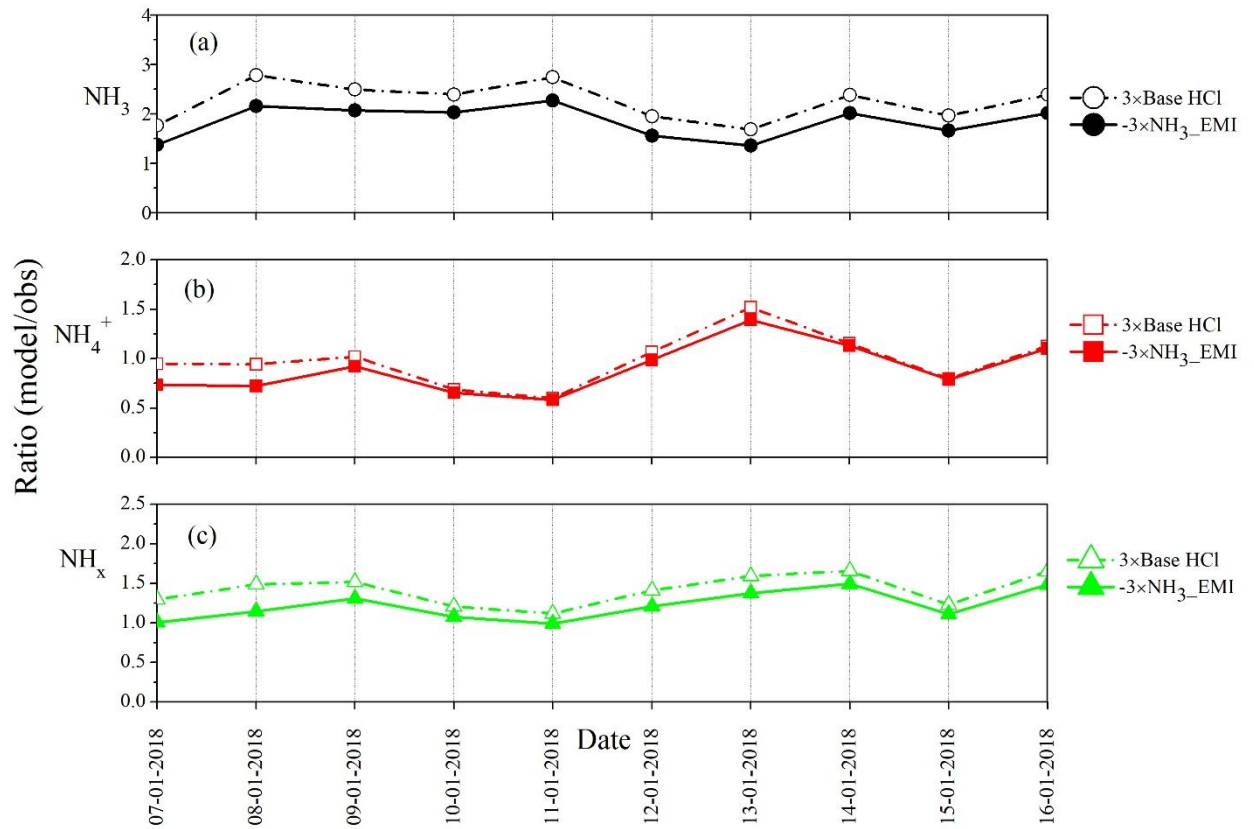
1041

1042

1043

1044

1045

1046

1047

1048

1049